PHYSICAL REVIEW LETTERS

VOLUME 7 JULY 15, 1961 NUMBER 2

STABLE PLASMA CONFINEMENT BY MULTIPOLE FIELDS*

T. Ohkawa† and D. W. Kerst

John Jay Hopkins Laboratory for Pure and Applied Science,
General Atomic Division of General Dynamics Corporation, San Diego, California

(Received June 5, 1961; revised manuscript received June 29, 1961)

Multipole magnetic fields increase with distance from and are convex toward the center of symmetry, providing a central equilibrium position and correct field curvature for stability of confined plasma. Braginskii and Kadomtsev[1] and Grad[2] have treated stability only for this convex portion of field, and Tuck[3] pointed out the utility of joining lines of force exterior to the multipole conductors to eliminate plasma escape along lines of force.

We describe a multipole configuration for which it has been possible to derive the conditions for plasma stability over the completely contained tubes of flux. These conditions can conveniently be met. The structure has only r and θ fields; thus eliminating the z field of Stellarators and pinches, and critical surfaces which break up into multiple pressure-reducing flux bundles under the influence of field errors.[4] A large volume of high $\beta(\equiv 2p/B^2)$ plasma is contained with no plasma surfaces in the sense of the cusp model.[1-3] The configuration is stable due to the externally supplied fields alone, no matter how little plasma is present. There is no requirement for persistence of special plasma current distribution as employed in pinches.

Figure 1 shows the cross section of a multipole field configuration. The z direction can be linear or along the circumference of a torus. Toroidal effects were found sufficiently small to be omitted in the calculations. Current flows in one direction through the rods and in the opposite direction on the wall. Briefly, the stability of the exterior of the multipole results from the flux tube connection between Region I where the field is convex toward the plasma, thus providing stability, and Region II where the field outside the plasma is concave toward the plasma contributing instability to the flux tube. The plasma on flux lines which circle a rod is in a completely stable situation. Conditions for net stability follow from the considerations sketched below which will be fully published elsewhere.

The energy principle[5] is used with the flux function, ψ, and orthogonal coordinate, χ, chosen so that

$$B_\theta = -\partial\psi/\partial r,$$

$$B_r = (1/r)(\partial\psi/\partial\theta),$$

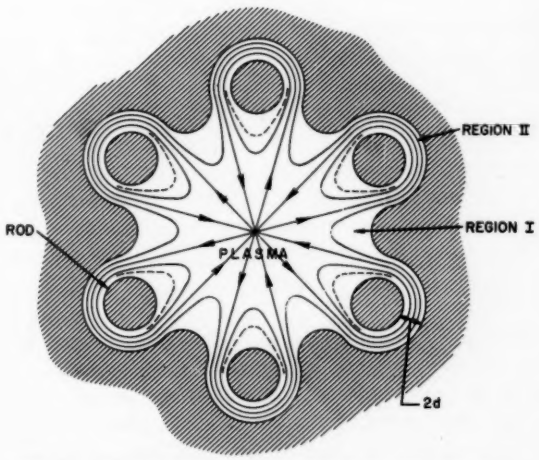

FIG. 1. Cross section of multipole configuration.

and so that a line element, ds, is

$$(ds)^2 = (1/B^2)(d\psi)^2 + J^2B^2(d\chi)^2 + (dz)^2.$$

We minimize the energy, δW, with respect to displacements in the χ and z directions, eliminating terms containing these components. The sufficient condition for stability that results is that the function,

$$S = \oint d\chi \{B^{-2}J^{-1}(\partial X_k/\partial\psi)^2 - X_k^{\,2}JB^{-2}(\partial p/\partial\psi)[\partial(p+\tfrac{1}{2}B^2)/\partial\psi]\},$$

be positive for all flux lines, where X_k is defined by

$$\xi_\psi = \sum_{k=0} (1/B)X_k \cos kz,$$

and ξ_ψ is the ψ component of the displacement. Consider first a uniform X_k along the arcs in Fig. 2. Then the stability condition becomes

$$(B_1^{\,2}/B_2^{\,2}) < \phi_1/\phi_2.$$

This condition is easy to satisfy since B_1 may be an order of magnitude less than B_2.

A worse displacement is one which does not occur in Region I where stability is provided, but rather the displacement is only in Region II. Stability would then have to come from bending the lines of force. The stability condition for this type of displacement is

$$(dp/dr_2) < (B_2^{\,2}/2r_2)(\pi/\phi_2)^2,$$

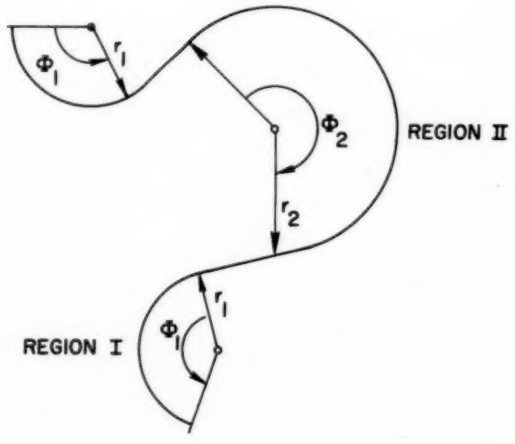

FIG. 2. Geometry of flux line for stability calculation.

or approximately

$$\beta_2 < (d/r_2)(\pi/\phi_2)^2.$$

This condition can also be satisfied with convenient proportions of rod and rod cavity.

A general result for plasma containment time is

$$\tau \sim \psi_{\max}^{\,2}/(\eta P_0),$$

where η is plasma resistivity in emu, or

$$\tau = 10^{-7} T_{ev}^{\,3/2} d^2 (B_2/B_1)^2 \text{ seconds}.$$

This time is generally long compared to the time for other processes to affect the plasma.

Even at low density and in the collisionless case, pressure is scalar and constant along a field line. A spherically symmetric velocity distribution in the central low field is maintained in the high-field region where the orbit magnetic moment is an invariant. In case the ion gyroradius is less than d, electrostatic ion reflection due to electron space charge occurs in the high-field region and in this case the action is invariant. This insures constancy of pressure on the central field line.

A free rod can have a stable equilibrium position, but with supports for the toroidal case, plasma lifetimes useful for some purposes are possible.

Linear arrays allow rods to be connected outside the plasma. Termination in a point cusp requires the cusp flux to join the rod flux and to wind its way along the multipole, producing a B_z. There is a confluence of cusp flux, as it starts around the rod, where a singular line is generated.

Injection of plasma through the convex surface of Region I allows entry by the instability caused by reversal of the pressure gradient.[6] Once within, the plasma is confronted with a stable configuration which confines it.

*This work was supported by General Atomic and Texas Atomic Energy Research Foundation.

†On leave from the University of Tokyo, Tokyo, Japan.

[1]S. Braginskii and B. Kadomtsev, Plasma Physics and the Problem of Controlled Thermonuclear Reactions (Pergamon Press, New York, 1961), Vol. III, p. 356.

[2]J. Berkowitz et al., Proceedings of the Second United Nations International Conference on the Peaceful Uses of Atomic Energy, Geneva, 1958 (United Nations, Geneva, 1958), Vol. 31, p. 171.

[3]J. L. Tuck, Nature 187, 863 (1960).

[4]T. Ohkawa and D. W. Kerst, Bull. Am. Phys. Soc. 6, 290 (1961).

[5]W. Bernstein, E. A. Frieman, M. D. Kruskal, and R. Kulsrud, Proc. Roy. Soc. (London) A244, 17 (1957).

[6]J. L. Tuck, Phys. Rev. Letters 3, 314 (1959).

EXPERIMENTAL EVIDENCE FOR QUANTIZED FLUX IN SUPERCONDUCTING CYLINDERS*

Bascom S. Deaver, Jr., and William M. Fairbank
Department of Physics, Stanford University, Stanford, California
(Received June 16, 1961)

We have observed experimentally quantized values of magnetic flux trapped in hollow superconducting cylinders. That such an effect might occur was originally suggested by London[1] and Onsager,[2] the predicted unit being hc/e. The quantized unit we find experimentally is not hc/e, but $hc/2e$ within experimental error.[3]

Although the unit of quantized flux is small ($hc/2e = 2.07\times10^{-7}$ gauss cm^2), it can be produced by a magnetic field easily measured and controlled in the laboratory if the area to which it is confined is sufficiently small. For our samples, one flux unit corresponds to a magnetic field of the order of 0.1 gauss. Measurements were made on two hollow tin cylinders. Cylinder No. 1 was 0.8 cm long, 2.33×10^{-3} cm outside diameter and 1.33×10^{-3} cm inside diameter. Cylinder No. 2 was 0.9 cm long, 1.64×10^{-3} cm outside diameter and 1.35×10^{-3} cm inside diameter. These were fabricated by electroplating tin on a one-centimeter portion of a No. 56 copper wire. The sample, plus protruding wire, was jacketed for protection and strength with electroplated copper to an approximate outside diameter of 8×10^{-3} cm.

A field-free region ($H = 0 \pm 0.001$ gauss) is prepared using three orthogonal Helmholtz coils. The tin cylinder is placed in this region and cooled through the superconducting transition in the presence of a known applied axial magnetic field. The net flux in the cylinder is measured both with the field on and after the field is turned off. The measurement is made by moving the tin cylinder up and down one hundred times per second with an amplitude of one millimeter and observing the electrical pickup in two small coils, each of ten thousand turns, surrounding the ends of the cylinder. The instrument is similar in concept to that described by Foner.[4] The induced emf measures the difference in the flux contained within the area of the cylinder and that which would have been in the same area if the cylinder were absent (or in the normal state). The system is calibrated by cooling the sample below the superconducting transition in zero field and observing the signal from the completely diamagnetic cylinder when a known magnetic field is applied. From the value of the field and the measured cross-section area of the cylinder, the absolute value of the flux for a given signal is calculated.

The diameter of each cylinder was measured with a microscope equipped with a micrometer eyepiece. X-ray photographs verified the dimensions of the tin cylinder after the application of the copper jacket. For the purpose of calculating flux, the measured radii of the cylinders are reduced by 0.6 micron due to an expected loss of superconducting properties on the surface of the tin in contact with the copper.[5] That this correction was approximately valid is indicated by a 0.2°K decrease in the value of the transition temperature for the sample No. 2 whose cylindrical walls were 1.5 microns thick, leaving, we believe, only 0.3 micron of superconducting material in the center after allowance for the effect of the center copper wire and the outside copper jacket. This is in agreement with the experimental results on electroplated tin.[5]

With this adjustment, the area used for the diamagnetic calibration of cylinder No. 1 is 3.84×10^{-6} cm^2, and the area of the hole is 1.65×10^{-6} cm^2. For cylinder No. 2 the corresponding quantities are 1.81×10^{-6} cm^2 and 1.70×10^{-6} cm^2.

Data on sample No. 1 are shown in Fig. 1, and on sample No. 2 in Fig. 2. The diagonal line through the origin represents the calibration. It is the signal corresponding to zero flux in the cylinder and hole in the presence of the applied field as described above. The experimental points shown on the graph represent two types of data for each value of the applied field. The points on the bottom half of each graph represent the signal in the presence of the applied field after cooling through the transition in that field. The points in the upper half represent the trapped flux after the field is subsequently reduced to zero. For each point in the lower curve there is a corresponding point in the upper curve. The solid lines represent calculated integral values of $hc/2e$.

It can be seen that certain features of the data are common to both samples. (1) Below a certain value of applied field, the total cross section of the cylinder acts as a perfect diamagnet, excluding all the flux, and no flux is trapped when the applied field is turned off. (We believe this

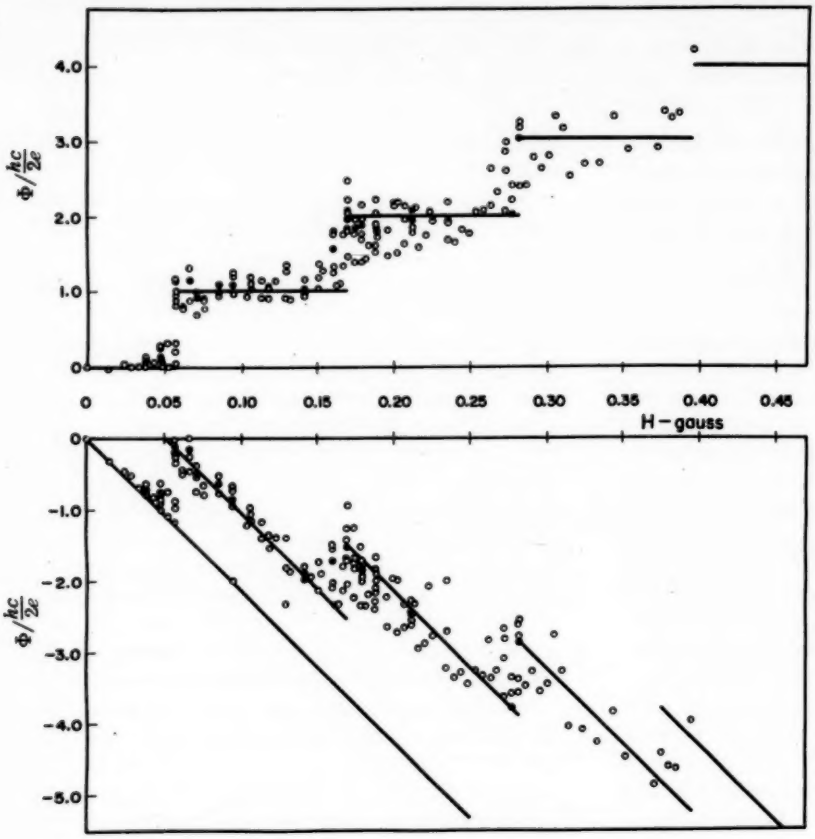

FIG. 1. (Upper) Trapped flux in cylinder No. 1 as a function of magnetic field in which the cylinder was cooled below the superconducting transition temperature. The open circles are individual data points. The solid circles represent the average value of all data points at a particular value of applied field including all the points plotted and additional data which could not be plotted due to severe overlapping of points. Approximately two hundred data points are represented. The lines are drawn at multiples of $hc/2e$. (Lower) Net flux in cylinder No. 1 before turning off the applied field in which it was cooled as a function of the applied field. Open and solid circles have the same significance as above. The lower line is the diamagnetic calibration to which all runs have been normalized. The other lines are translated vertically by successive steps of $hc/2e$.

provides a way of obtaining a truly zero-magnetic-field region.) (2) When the applied field exceeds a certain value, flux is trapped both with the field on, and after the applied field is turned off. The amount of this trapped flux within the experimental accuracy of the data is $hc/2e$.

The amount of trapped flux remains constant as the applied field is increased until a value approximately three times that for the initial trapping is reached, at which point the trapped flux increases to about twice the original amount. There appears to be evidence for additional changes at five and seven times the field for the first trapping.

Fluctuations in the data are caused by variations in the zero of the magnetic field, changes in the gain, vibration amplitude, drift, and random noise in the detection system. The approximately two hundred data points for sample No. 1 were taken over a three-week period during which the drift and noise were gradually improved. The fluctuations of the data around the values 0 and $hc/2e$ represent, we believe, expected scatter from drift and noise. This scatter has been greatly improved for sample No. 2. For both samples the data are consistent with values 0 and $hc/2e$ for the trapped flux as described above.

Near the transition to the second and third steps the fluctuations in the data are greater, and in addition points lie between the steps. Some increased scatter is expected since the absolute fluctuations due to changes in gain and vibration amplitude are proportional to the size of the signal. The points between the steps do not necessarily indicate trapping of nonintegral values of flux. Since the observed signal is the sum of the emf's from coils at the two ends of the sample, a flux line passing out of the cylinder at some point other than the end may produce different signals in the two coils. The two ends of the cylinder are not quite identical; so near the transition region it is probable that the two ends might trap a different number of units

of flux, the extra unit being shoved out the side of the cylinder. This is especially probable for sample No. 1 since the x-ray photograph showed a break in the tin coating near the middle of the cylinder. Also, it is known that flux can create a normal region in a superconductor by shrinking in size until the critical field is exceeded. In this experiment we were unable to measure independently the signals from the two coils. However, in future experiments this will be done to remove this ambiguity. It is interesting to note that no intermediate points are found outside the expected scatter of the data near the first step. One point for which no flux was trapped was found near the center of the first step with sample No. 1.

In conclusion, we find:

1. The flux trapped in a superconducting cylinder both in the presence and absence of an applied magnetic field is not continuous but exhibits a step behavior, the first step occurring for $\Phi = hc/2e$, within experimental error in the data. Considering all sources of error, we estimate that the value of the trapped flux at the first step is $hc/2e \pm 20\%$. If the correction to the size of the cylinder due to the presence of the copper should prove invalid, an additional 11% error could arise for the large cylinder and 17% for the small cylinder.

2. The data seem to indicate additional steps at hc/e, $3hc/2e$, and $2hc/e$. The points appearing between these levels will be investigated further.

3. The ratio of the fields at which the steps occur are approximately 1, 3, 5, and 7. In the first cylinder (for which the effective cross-sectional area of the cylinder is 2.33 times the area of the hole), the first jump occurs when the flux passing through the total effective cross section of the cylinder in the normal state is approximately $hc/2e$.

For cylinder No. 2 (in which the effective cross-sectional area of the cylinder is 1.1 times the area of the hole), the first jump occurs when the flux passing through the total effective cross section of the cylinder in the normal state is approxi-

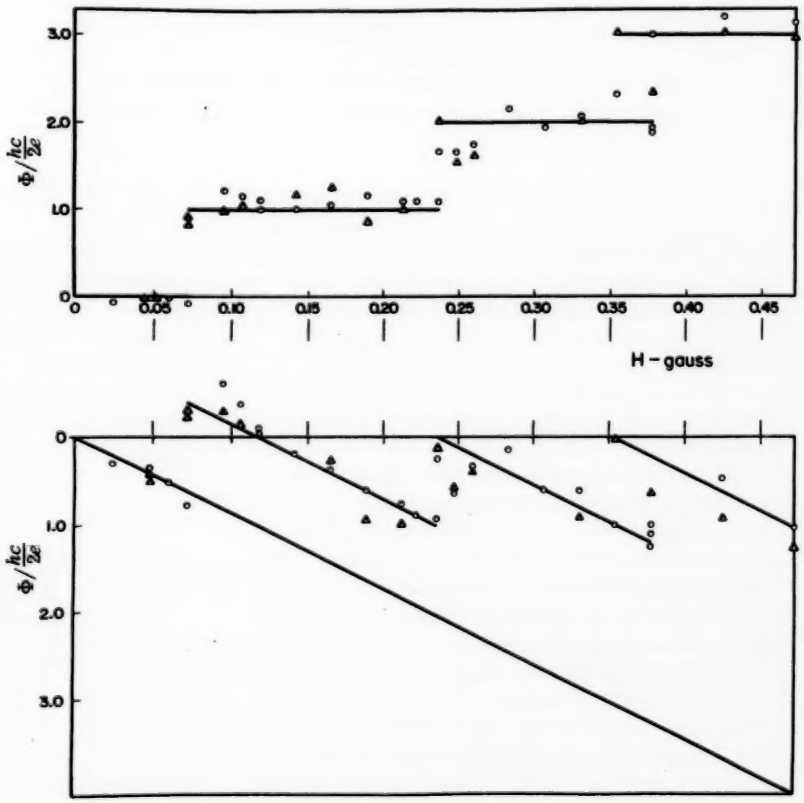

FIG. 2. (Upper) Trapped flux in cylinder No. 2 as a function of magnetic field in which the cylinder was cooled below the superconducting transition temperature. The circles and triangles indicate points for oppositely directed applied fields. Lines are drawn at multiples of $hc/2e$. (Lower) Net flux in cylinder No. 2 before turning off the applied field as a function of the applied field. The circles and triangles are points for oppositely directed applied fields. The lower line is the diamagnetic calibration to which all runs have been normalized. The other lines are translated vertically by successive steps of $hc/2e$.

mately $0.6hc/2e$. In a following Letter, Byers and Yang[6] conclude that in a thin ring the first jump should occur at $0.5hc/2e$.

4. Since the time constant of our measuring circuit is 25 seconds, this experiment gives only a large upper limit for the time involved in reaching these quantized flux values. Mercereau and Vant-Hull[7] have reported a negative experiment designed to observe quantized flux in a 1-mm ring cooled 6000 times per second through the superconducting transition in a small magnetic field. It is possible that the difference in their results and the results of our experiment are due to a minimum time necessary to establish equilibrium. We are planning to investigate this relaxation time.

We have had the pleasure of discussing the results of this experiment with N. Byers, C. N. Yang, and L. Onsager, whose interpretation of these results appear in the following Letters.[6,8] One of us (WMF) also wishes to acknowledge his indebtedness to F. London and M. J. Buckingham who greatly influenced his concept of the superfluid state. We also wish to thank F. Bloch, L. I. Schiff, and J. D. Bjorken for many stimulating discussions of the experiment. We wish to acknowledge the invaluable assistance of M. B. Goodwin.

---

*Work supported in part by grants from the National Science Foundation, the Office of Ordnance Research (U. S. Army), and the Linde Company.

[1]F. London, Superfluids (John Wiley & Sons, New York, 1950), p. 152.

[2]L. Onsager, Proceedings of the International Conference on Theoretical Physics, Kyoto and Tokyo, September, 1953 (Science Council of Japan, Tokyo, 1954), pp. 935-6.

[3]Such a possibility was mentioned by Lars Onsager to one of us (WMF) at the conference on superconductivity in Cambridge, England, 1959 (unpublished).

[4]S. Foner, Rev. Sci. Instr. 30, 548 (1959).

[5]E. Burton, H. Grayson-Smith, and J. Wilhelm, Phenomena at the Temperature of Liquid Helium (Reinhold Publishing Corporation, New York, 1940), p. 120.

[6]N. Byers and C. N. Yang, following Letter [Phys. Rev. Letters 7, 46 (1961)].

[7]J. E. Mercereau and L. L. Vant-Hull, Bull. Am. Phys. Soc. 6, 121 (1961).

[8]L. Onsager, this issue [Phys. Rev. Letters 7, 50 (1961)].

THEORETICAL CONSIDERATIONS CONCERNING QUANTIZED MAGNETIC FLUX IN SUPERCONDUCTING CYLINDERS*

N. Byers and C. N. Yang†

Institute of Theoretical Physics, Department of Physics, Stanford University, Stanford, California

(Received June 16, 1961)

In a recent experiment,[1] the magnetic flux through a superconducting ring has been found to be quantized in units of $ch/2e$. Quantization in twice this unit has been briefly discussed by London[2] and by Onsager.[3] Onsager[4] has also considered the possibility of quantization in units $ch/2e$ due to pairs of electrons forming quasi-bosons.

The previous discussions[3] leave unresolved the question whether quantization of the flux is a new physical principle or not. Furthermore, sometimes the discussions seem[2] to be based on the assumption that the wave function of the superconductor in the presence of the flux is proportional to that in its absence, an assumption which is not correct. We shall show in this Letter that (i) no new physical principle is involved in the requirement of the quantization of magnetic flux through a superconducting ring, (ii) the Meissner effect is closely related to the requirement that the flux through any area with a boundary lying entirely in superconductors is quantized, and (iii) the quantization of flux is an indication of the pairing of the electrons in the superconductor.

Macroscopic discussion. Consider a multiply connected superconducting body P with a tunnel O (Fig. 1). We shall only discuss macroscopic

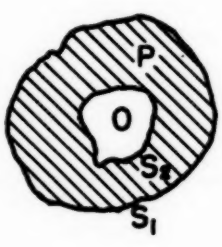

FIG. 1. Multiply connected superconductor.

dimensions much larger than the penetration depth. The Meissner effect then states that inside the superconductor P the magnetic field is zero, and the current is zero. Surface currents, however, do exist and persist on the surfaces S_1 and S_2. The surface currents and the external sources of magnetic fields together produce no magnetic flux in the interior P of the superconductor. They in general, however, produce a net magnetic flux through O, to be denoted by Φ.

The energy eigenfunction ψ of the electrons in the superconductor satisfies

$$\sum_j \frac{1}{2m}\left[-i\hbar\vec{\nabla}_j + \frac{e}{c}\vec{A}(\vec{r}_j)\right]^2\psi + V\psi = E\psi, \qquad (1)$$

where $\vec{A}$ is the vector potential due to the surface currents and external magnetic sources. Inside P,

$$\vec{\nabla}\times\vec{A} = 0.$$

Hence $\vec{A} = \vec{\nabla}\chi$, where χ is not single valued in P but increases by

$$\Delta\chi = \oint \vec{A}\cdot d\vec{l} = \iint \vec{H}\cdot d\vec{\sigma} = \Phi, \qquad (2)$$

whenever one goes around the tunnel O once. Defining

$$\psi' = \psi \exp\sum_j i\frac{e}{c\hbar}\chi(\vec{r}_j), \qquad (3)$$

we see that (1) reduces to

$$\sum_j \frac{1}{2m}(-i\hbar\vec{\nabla}_j)^2\psi' + V\psi' = E\psi'. \qquad (4)$$

The vector potential $\vec{A}$ is eliminated from this equation. However, the boundary condition for ψ' is that when all electron coordinates are fixed, except for one, $\vec{r}_l$, and $\vec{r}_l$ is brought around O once, ψ' changes by a constant factor

$$\psi' \to \psi' e^{i(e/c\hbar)\Phi}. \qquad (5)$$

[To prove (5) we use (3) and (2) and the fact that ψ is single valued.]

The eigenvalues E are determined by the differential equation (4) and the boundary condition (5). It is thus obvious that we have:

Theorem 1. The energy levels are periodic in the magnetic flux Φ with a period ch/e.

If the surfaces S_1 and S_2 are concentric cylinders on which $\psi = 0$, and V is put equal to zero, the energy levels E can be explicitly solved for, illustrating this theorem. One notices that ψ' is not simply proportional to $\psi(\Phi = 0)$, as is sometimes[2] assumed in the literature.

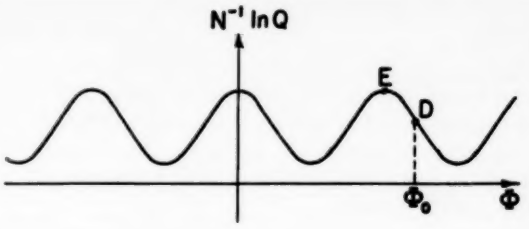

FIG. 2. Periodic variations in $N^{-1}\ln Q$ as a function of trapped flux Φ.

If V is a real function of r_j, by taking the complex conjugate of (4) and (5), we have:

Theorem 2. The energy levels are even functions of Φ.

It is clear that theorems 1 and 2 remain valid if we introduce the lattice coordinates of the metal and if we introduce the spin of the electrons. The operation of complex conjugation in the proof of theorem 2 has then to be replaced by the time reversal operation and the proof depends on the time reversal invariance of the interactions.

From these theorems it follows trivially that:

Theorem 3. The partition function Q of the system is an even periodic function of Φ with period ch/e.

At $\Phi = (ch/2e)\times$integer, this theorem shows that

$$\partial \ln Q/\partial\Phi = 0, \qquad (6)$$

and that $\ln Q$ has the general form shown in Fig. 2.

Now the body current in the superconductor around O is

$$I = kTc\,\partial \ln Q/\partial\Phi. \qquad (7)$$

(c = velocity of light.) In the differentiation we keep the temperature T constant.

The Meissner effect requires that $I = 0$. Thus the equilibrium states are given by the maxima and minima on the curve in Fig. 2. We shall now give an argument to show that the maxima, not the minima, are the equilibrium states realized. A point D in Fig. 2 is not an equilibrium state so the calculation of the partition function at that point is strictly speaking meaningless. But the slope of the curve at that point indicates that if a flux Φ_0 is made to pass through O, a body current would be induced, the sense of the current being negative according to (7). The additional flux due to this body current causes the flux through O to decrease. The equilibrium state reached would therefore be E

which is a maximum of the curve. We state this as:

Theorem 4. The superconducting state is given by the maxima of $\ln Q$ as a function of Φ.

If the external flux does not assume a value for which $\ln Q$ is a maximum, surface currents will flow on S_1 and S_2 to make up a total flux Φ for which $\ln Q$ is a maximum.

The experiment of reference 1 and theorem 4 together prove that $\ln Q$ has maxima at integral values of $\Phi/(ch/2e)$. Whether a microscopic theory yields these maxima will be discussed in the next section. If it does, then theorem 4 shows the following: The flux through any surface whose boundary loop lies entirely in superconductors is quantized in units $ch/2e$. The requirement of this quantization in turn clearly implies that the flux through any small area in a superconductor is zero; hence it implies the Meissner effect.

In a loose sense the above argument can be used to "derive" the Meissner effect itself: If the magnetic flux in a superconductor is not zero, body currents will flow around all loops through which the flux is not quantized. The system cannot reach a steady state until all magnetic flux is expelled from the interior of the superconductor.

Microscopic considerations. We now want to see whether a microscopic calculation does or does not lead to maxima of $\ln Q$ at $\Phi/(ch/2e)$ = integer.

To investigate this point we first take a collection of noninteracting spinless electrons between two concentric cylinders S_1 and S_2. The electrons at a point at a distance r from the axis have momenta p_r, p_θ, and p_z in the radial, azimuthal, and z directions. Clearly

$$p_\theta r = n\hbar. \quad (n = \text{integer})$$

The energy of the electron is

$$\frac{1}{2m}\left[p_r^2 + p_z^2 + \frac{\hbar^2}{r^2}\left(n + \frac{e}{ch}\Phi\right)^2\right]. \tag{8}$$

The partition function Q can be computed from such an energy spectrum. The resultant $N^{-1}\ln Q$ [to the order N^0] does not depend on Φ. Thus, according to theorem 4, for a collection of noninteracting electrons, the flux in the tunnel does not have to be quantized.

It is not difficult to understand why for such a model $N^{-1}\ln Q$ does not depend on Φ. To see this we suppress the p_r and p_z degrees of freedom and take the temperature $T = 0$. The one-dimensional Fermi sea problem,

$$\frac{\hbar^2}{2mr^2}\sum\left(n + \frac{e}{ch}\Phi\right)^2,$$

gives an average energy per particle of

$$\frac{E}{N} = \text{constant} + \frac{\hbar^2}{2mr^2}\frac{e^2}{c^2\hbar^2}\Phi^2, \quad \left|\frac{e\Phi}{ch}\right| \leq \tfrac{1}{2}, \tag{9}$$

if $N \equiv$ the number of particles is odd. But if N is even, then

$$\frac{E}{N} = \text{constant} + \frac{\hbar^2}{2mr^2}\left(\frac{e\Phi}{ch} - \tfrac{1}{2}\right)^2, \quad \tfrac{1}{2} \geq \frac{e\Phi}{hc} \geq 0 \tag{10}$$

$$= \text{constant} + \frac{\hbar^2}{2mr^2}\left(\frac{e\Phi}{ch} + \tfrac{1}{2}\right)^2, \quad 0 \geq \frac{e\Phi}{hc} \geq -\tfrac{1}{2}. \tag{10'}$$

Thus, depending on the evenness or oddness of N, the energy has a minimum at $e\Phi/ch = \frac{1}{2}$ or 0 (modulo 1). The three-dimensional problem at $T = 0$ is decomposable into many one-dimensional problems with varying values of N. Thus the above-discussed fluctuation leads to a cancellation for the three-dimensional problem, resulting in an $N^{-1}\ln Q$ versus Φ curve that is flat. (An $N^{-1}\ln Q$ curve that is flat applies to the case of a metal in its normal rather than superconducting state.) A similar cancellation obtains for $T \neq 0$.

In the neighborhood of $\Phi = +0$ the states with $n > 0$ have energies that increase with Φ, and those with $n < 0$ have energies that decrease with Φ. The average energy for the two states n and $-n$, however, increases with Φ like

$$\text{constant} + (\hbar^2/2mr^2)(e\Phi/ch)^2. \tag{11}$$

If there is a "pair correlation" of the kind proposed by Bardeen, Cooper, and Schrieffer[5] for the superconductor so that states n and $-n$ (or a pair of time-reversed states) are either both occupied or both unoccupied, (11) becomes the correct energy per particle for small Φ. (In such a case the fluctuation and cancellation phenomena disappear.) This is represented in Fig. 3 by the parabolas at $2e\Phi/ch = -2, 0, 2,$ etc.

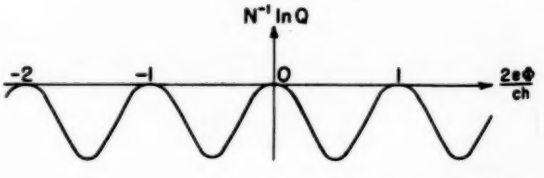

FIG. 3. A curve of $N^{-1}\ln Q$ versus $2e\Phi/ch$, showing parabolic behavior near maxima at $2e\Phi/ch$ = integer.

At $2e\Phi/ch = 1$, pairing between

$$n + \frac{e}{hc}\Phi = n + \tfrac{1}{2} = \tfrac{1}{2} \text{ and } -\tfrac{1}{2},\ \tfrac{3}{2} \text{ and } -\tfrac{3}{2},\ \text{etc.},$$

occurs and the energy per particle remains the same as for the case $\Phi = 0$ (to order N^0). In the neighborhood of $2e\Phi/ch = 1$, the additional energy for each of these pairs is again twice

$$(\hbar^2/2mr^2)[(e\Phi/ch) - \tfrac{1}{2}]^2,$$

which give rise to the parabolas at $2e\Phi/ch = \pm 1$ in Fig. 3. In the absence of a detailed theory, we draw a smooth curve in Fig. 3 to extrapolate between the maxima.

Thus the Bardeen, Cooper, Schrieffer pairs for the superconducting state give rise to the curves such as those depicted in Fig. 3, where the parabolas are repeated at periods $\Delta(2e\Phi/ch) = 1$, and the central parabola is given by

$$N^{-1}\ln Q = -\frac{f}{kT}\frac{\hbar^2}{2m\langle r^2\rangle_{\text{av}}}\left(\frac{e\Phi}{ch}\right)^2 + \text{constant}, \qquad (12)$$

where f = fraction of electrons that are paired.

It is interesting to estimate the magnitude of the body current at, say,

$$0 < 2e\Phi/ch < \tfrac{1}{2}. \qquad (13)$$

It is, by (7),

$$I = -Nfc(e^2/mc^2)\Phi/(4\pi^2\langle r^2\rangle_{\text{av}}).$$

The flux induced by this current is, for a thin ring superconductor,

$$\Phi_{\text{induced}} = -f \times (\text{number of electrons in a length } e^2/mc^2 \text{ of the ring})\Phi.$$

For the experiment of reference 1, $-\Phi_{\text{induced}}/\Phi \gg 1$ if f is not too small, showing that the maxima in Fig. 3 are very pronounced.

From Fig. 3 and the argument preceding theorem 4, we conclude that the trapped flux Φ and the original flux Φ_0 are related in the following way:

$\Phi_0/(ch/2e)$	Φ
$-\frac{1}{2} \to \frac{1}{2}$	0
$\frac{1}{2} \to \frac{3}{2}$	1
$\frac{3}{2} \to \frac{5}{2}$	2
etc.	

It is interesting to notice that the existence of the variation of the energy levels of the electrons in P with the flux Φ, even when there is no magnetic field in P, is based on the same principle as the experiment proposed by Aharonov and Bohm.[6,7]

We wish to thank W. M. Fairbank and B. Deaver for informing us of the progress of their beautiful experiment and for many discussions. We also wish to thank F. Bloch for stimulating discussions. One of us (CNY) takes this opportunity to thank the members of the Physics Department of Stanford University for the hospitality extended him during his visit.

---

*Work supported in part by the U. S. Air Force through the Air Force Office of Scientific Research.

†Permanent address: Institute for Advanced Study, Princeton, New Jersey.

[1]B. S. Deaver, Jr., and W. M. Fairbank, preceding Letter [Phys. Rev. Letters 7, 43 (1961)].

[2]F. London, Superfluids (John Wiley & Sons, Inc., New York, 1950), p. 152.

[3]L. Onsager, Proceedings of the International Conference on Theoretical Physics, Kyoto and Tokyo, September, 1953 (Science Council of Japan, Tokyo, 1954), pp. 935-6.

[4]L. Onsager (private communication to W. M. Fairbank).

[5]J. Bardeen, L. N. Cooper, and J. R. Schrieffer, Phys. Rev. 108, 1175 (1957).

[6]Y. Aharonov and D. Bohm, Phys. Rev. 115, 485 (1959).

[7]R. G. Chambers, Phys. Rev. Letters 5, 3 (1960).

MAGNETIC FLUX THROUGH A SUPERCONDUCTING RING

Lars Onsager*
University of California, La Jolla, California
(Received June 15, 1961)

London[1] recognized that the magnetic flux embraced by a superconducting ring ought to be quantized. He argued as follows: The current density is proportional to the average of

$$\vec{p} - (Q/c)\vec{A},$$

where $\vec{A}$ denotes the vector potential and Q the charge of the current-carrying particle. In the interior of the superconductor the current density vanishes, so that the condition

$$\oint \vec{p} \cdot d\vec{x} = -nh$$

for a single-valued wave function implies

$$\Phi = \oint \vec{A} \cdot d\vec{x} = -nhc/Q.$$

Substituting $Q = -e$ for the charge of the electron, he arrived at the conclusion

$$\Phi = nhc/e.$$

It is possible to recast London's discussion in a form which is completely Lorentz and gauge invariant; the details need not concern us here.

London's result inspired the suggestion[2] that the quantization of flux might be an intrinsic property of the electromagnetic field.

Not much later, Schafroth[3] pointed out that electron pairs held together by attractive interactions would obey Bose statistics and be capable of superfluid (Einstein) condensation. A likely source of the requisite attractive interaction—by way of the phonon field—had been suggested by Fröhlich[4] and by Bardeen.[5] These ideas form the basis of more detailed theories, which explain the various observed properties of superconductors so well that they have been generally accepted.

Deaver and Fairbank[6] have found that the flux embraced by a superconducting annulus varies in steps of half the size proposed by London. This is readily explained by Schafroth's theory, which requires

$$Q = -2e,$$
$$\Phi = nhc/2e.$$

The discovery of steps just this size provides a convincing direct proof for the pairing of electrons.

The notion that the electromagnetic field itself might be subject to a similar condition seems untenable now, for singly charged bosons exist (deuterons) and a condition imposed on the electromagnetic field ought to be equally compatible with all charged particles.

Instead, we arrive at the remarkable result that we can measure the magnetic flux (except for an additive undetermined multiple of $hc/2e$) embraced by a given closed path without examining the enclosed field; a superconductor placed along the path will respond with a supercurrent which compensates the fractional excess of flux. Complete Meissner effect in a multiply-connected superconductor requires coherent ring closure. We may infer that such closure will not take place unless the free energy liberated by the matching of phases exceeds the kinetic energy of the necessary supercurrent plus the added magnetic field energy. The detailed kinetic mechanism is not yet known.

I am indebted to F. Bloch for a discussion which clarified the closure problem, and to B. Deaver and W. M. Fairbank for the communication of their unpublished results.

---

*Permanent address: Sterling Chemistry Laboratory, Yale University, New Haven, Connecticut.

[1]F. London, Superfluids (John Wiley & Sons, Inc., New York, 1950), Vol. 1, p. 152.

[2]L. Onsager, Proceedings of the International Conference on Theoretical Physics, Kyoto and Tokyo, September, 1953 (Science Council of Japan, Tokyo, 1954), p. 935.

[3]M. R. Schafroth, Phys. Rev. 96, 1149, 1442 (1954).

[4]M. Fröhlich, Phys. Rev. 79, 845 (1950); Proc. Roy. Soc. (London) A215, 291 (1952).

[5]J. Bardeen, Phys. Rev. 79, 167 (1950); 80, 517 (1950); 81, 829 (1951).

[6]B. Deaver and W. M. Fairbank, this issue [Phys. Rev. Letters 7, 43 (1961)].

EXPERIMENTAL PROOF OF MAGNETIC FLUX QUANTIZATION IN A SUPERCONDUCTING RING*

R. Doll and M. Näbauer
Kommission für Tieftemperaturforschung der Bayerischen Akademie der Wissenschaften, Herrsching/Ammersee, Germany
(Received June 19, 1961)

From theoretical considerations, based on wave mechanics, London[1] concluded that the magnetic flux frozen in in a twofold-connected superconducting body (ring or tube) should not have any arbitrary value, but only such values which are integer multiples of a basic unit ϕ_0,

$$\phi_0 = hc/e = 4.12\times10^{-7} \text{ gauss cm}^2. \quad (1)$$

That means the magnetic flux should be quantized. Bardeen and Schrieffer[2] also agreed with this conclusion.

In order to verify a possible flux quantization, the mechanical torque exerted by a magnetic field H_x on a small superconducting lead tube with frozen-in magnetic flux has been measured.

From the following equation, one obtains the magnetic field H_{y0} necessary to freeze in just one flux unit ϕ_0:

$$H_{y0} = \phi_0 \times (4/\pi d^2), \quad (2)$$

where d is the diameter of the tube. The diameter has to be chosen sufficiently small that the fluctuations of the earth's magnetic field can be neglected relative to the magnetic field adequate to freeze in one flux unit. This has been achieved with a tube of 10.3-micron diameter and 0.6-mm length (see Fig. 1), which gives a magnetic field of $H_{y0} = 0.5$ oe, according to Eq. (2).

The sample consists of a small lead cylinder, prepared by evaporating lead on a quartz fiber (of about 10-micron diameter and with a length of about 1 mm).

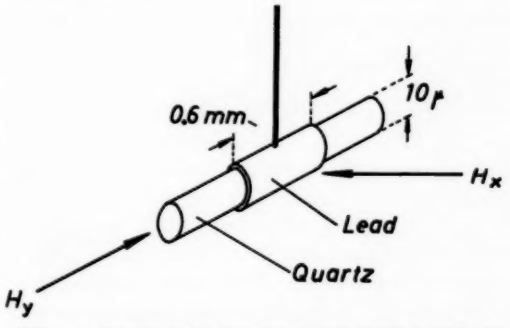

FIG. 1. Schematic diagram of the sample with the directions of the applied field H_y to be frozen in, and the measuring field H_x.

The very small torque, proportional to the frozen-in flux and to the measuring field H_x (normal to H_y), can be observed by an already known autoresonance method.[3,4] The sample is suspended on a thin torsion fiber (normal to H_y and H_x) inside a coil. In connection with a mirror for recording the oscillation amplitude it represents a system of damped torsion oscillation. The oscillation of the system can be kept at a constant amplitude by the alternating torque, caused by periodically reversing the magnetic field H_x of the coil. The oscillating system itself controls the time of switching the field by means of a photoelectric device. The damping of the system being known, the constant resonance amplitude is a measure for the torque which acts on the sample.

Each experimental value was obtained in the following manner: 1. The sample was heated above the transition temperature; then a defined field to be frozen in, H_y, was applied. 2. After recooling below the transition temperature, H_y was switched off. 3. The resonance amplitude was measured as described above.

The resonance amplitude is proportional to the product (measuring field H_x) times (magnetic moment of the sample). The latter in turn is proportional to the frozen-in flux. Figure 2 shows the measured resonance amplitude divided by the driving field H_x as a function of the field H_y. (H_x has always been about 10 oe.)

As Fig. 2 shows, it is impossible to freeze in any flux between $H_y = -0.1$ and $+0.1$ oe. Near ±0.1 oe there occur marked steps. Upon increasing the magnetic field H_y, the frozen-in fluxes remain nearly constant between 0.1 and 0.3 oe. At 0.3 oe another step occurs, again followed by a series of constant values.

This is exactly what is expected of a quantized magnetic flux in a twofold-connected superconducting body. If an arbitrary flux could be frozen in, the relation between magnetic flux and field H_y would be as shown in Fig. 2 by the dashed line. This has been obtained by measurements at comparatively high fields ($H_y = 10$ oe), in which case the value of one flux unit is already very small compared with the entire frozen-in flux.

With the microscopically measured diameter of

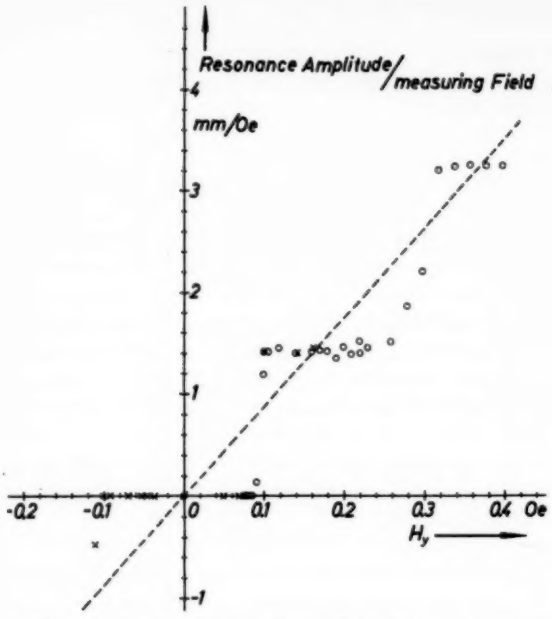

FIG. 2. Resonance amplitude divided by measuring field H_x as a function of the applied field H_y. The ordinate is proportional to the frozen-in flux. ×– First run; o– second run.

the lead tube, Eq. (2) predicts for the interval of the magnetic field strength corresponding to one flux unit a value of $H_y = 0.5$ oe. The experimentally observed interval, however, reaches only 0.2 oe, that is about 40% of the calculated value. So far the reason for this discrepancy is not clear. For example, an error of 60% in the determination of the lead tube's diameter would explain the difference, but such an error is improbable.

The experiments are being continued with higher fields H_y and other superconductors of various diameters.

Mercereau and Vant-Hull[5] also tried to verify London's postulate of the quantization of magnetic flux in a superconducting ring. The result of their experiments was negative.

The authors are indebted to Professor W. Meissner who made possible and promoted this work. The authors would further like to thank Professor F. X. Eder for encouragement and helpful discussions.

---

*Presented at the Conference on Fundamental Research in Superconductivity, IBM Research Center, Yorktown Heights, New York, June 15-17 (1961).

[1]F. London, Superfluids (John Wiley & Sons, New York, 1950), Vol. I, p. 152.

[2]J. Bardeen and I. R. Schrieffer, Progress in Low-Temperature Physics (North-Holland Publishing Company, Amsterdam, 1961), Vol. III, p. 182.

[3]A. Einstein and W. J. de Haas, Verhandl. deut. physik. Ges. 17, 152 (1915).

[4]R. Doll, Z. Physik 153, 207 (1958).

[5]J. E. Mercereau and L. L. Vant-Hull, Bull. Am. Phys. Soc. 6, 121 (1961).

EXPERIMENTAL DETECTION OF TRANSITION RADIATION*†

H. Boersch, C. Radeloff, and G. Sauerbrey

I. Physikalisches Institut of the Technische Universität Berlin, Berlin, Germany

(Received February 17, 1961)

If an electron approaches the boundary between vacuum and metal, a changing dipole field due to the electron and its image charge is formed which, according to the theory of Ginsburg and Frank,[1] effects the emission of "transition radiation." In the experiment electrons bombarding a metal surface generate a visible radiation known as "Lilienfeld radiation." The results of the experiments done before this work are, however, contradictory.[2-4] Therefore we undertook to exclude by more careful experiments the influence of surface contaminations and to compare the experimental Lilienfeld radiation with the theoretical transition radiation by variation of different parameters.

Our investigations were carried out at pressures of about 10^{-9} mm Hg with massive heatable targets and with condensed films of more than 1 μ thickness. The electron beam was produced by field emission and pulsed with a frequency of 100 kc/sec. The energy of the electrons was in general 2-12 kev. The intensity of the Lilienfeld radiation was measured with a photomultiplier tube and a phase discriminator. The results of our investigations are as follows:

(1) The intensity of the Lilienfeld radiation is independent of the temperature of the target.

The temperature range was 300°K to 2300°K for W targets, up to 1800°K for Ta and Mo, and up to 1300°K for Ti.

The intensity of the Lilienfeld radiation is also independent of the gas pressure, as investigated for tungsten in the range from 10^{-9} to 10^{-5} mm Hg. Consequently, if gas films are adsorbed on the surfaces, they have no influence. Therefore the Lilienfeld radiation is a property of the clean metal surface only, like the transition radiation.

(2) Like the transition radiation, the Lilienfeld radiation of W, Ta, Mo, Ti, and Pt is nearly plane polarized (Table I). The electric field vector is oscillating in the plane given by the normal to the target plane and the direction of observation. Its direction is independent of the angle of incidence of the electron beam. The degree of polarization for Ag and Cs is lower than that for the former metals. This decrease is probably caused by greater roughness of the surfaces.

(3) The intensities of the transition radiation and of the Lilienfeld radiation for W, Ni, Al, and Cu increase linearly with both electron energy and current density. The investigations ranged for electron energy from 6 to 30 kev and for current density from 0.1 to 10 ma/cm^2.

(4) The angular distributions of the Lilienfeld radiation for tungsten and of the transition radiation for a metal with a dielectric constant $|\epsilon| = 3$ are nearly identical from $\theta = 10°$ to $\theta = 60°$ (Fig. 1).

(5) The spectrum of the Lilienfeld radiation, recorded by a quartz spectrograph with a resolution $\Delta\lambda \sim 100$ A, forms a continuum (Fig. 2). The spectra of the Lilienfeld radiation and of the transition radiation for silver are plotted in Fig. 3. Both spectra nearly agree in the slow increase from red to blue and in the following abrupt decrease in the ultraviolet. The theoretical increase of the transition radiation at 3000 A

Table I. Degree of polarization P and efficiency $\eta_{\Delta\lambda}$ of the Lilienfeld radiation and of the transition radiation. Angle of observation $\theta = 65°$ against the normal of the target plane. The efficiency $\eta_{\Delta\lambda}$ is the ratio between the total power of the Lilienfeld radiation in the spectral range $\lambda = 4000$ to 5120 A, $\Delta\lambda = 1120$ A, and the power of the electron beam.

Metal	Lilienfeld radiation (exp.) P	Lilienfeld radiation (exp.) $10^9\eta_{\Delta\lambda}$	Transition radiation (theor.) P	Transition radiation (theor.) $10^9\eta_{\Delta\lambda}$
Tungsten	0.96	4	1.0	4.3
Tantalum	0.96	3.5	1.0	3.9
Molybdenum	0.96	4	1.0	4.3
Titanium	0.88	2	1.0	2.1
Platinum	0.92	5	1.0	5.1
Silver	0.6	8	1.0	5.7
Cesium	0.5	11	1.0	3.9

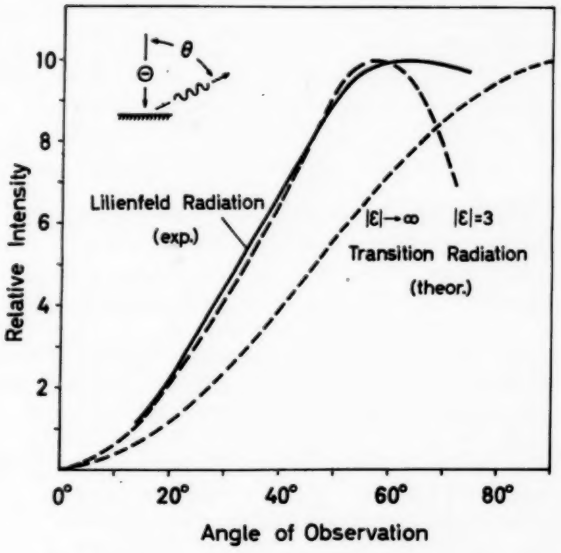

FIG. 1. Intensity of the investigated Lilienfeld radiation (solid line) for tungsten and of the calculated transition radiation (dashed line) versus the angle of observation. ϵ = dielectric constant.

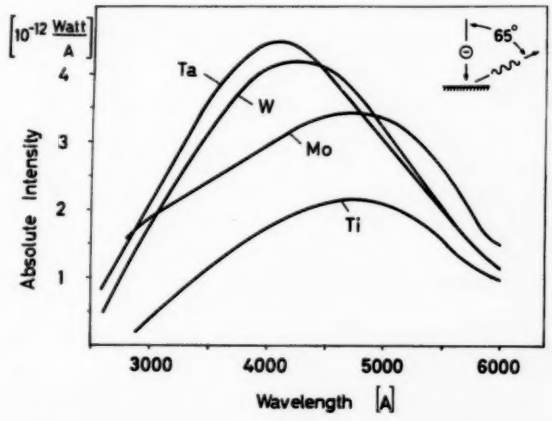

FIG. 2. Spectrum of the Lilienfeld radiation for Ta, W, Mo, and Ti. Absolute intensity relative to 1-watt electron beam power and to a range of wavelength $\Delta\lambda = 1$ A.

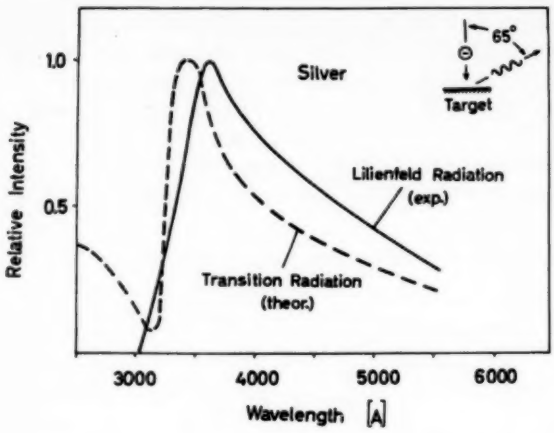

FIG. 3. Spectra of the Lilienfeld radiation (exp.) and the transition radiation (theor.) for silver.

is not reproduced by the experimental spectrum. It is probable that in this part of the spectrum the sensitivity of our apparatus is not sufficient.

(6) The efficiency $\eta_{\Delta\lambda}$ of the Lilienfeld radiation for W, Ta, Mo, Ti, and Pt agrees surprisingly well with the calculated efficiency of the transition radiation (Table I). The efficiency for the condensed metals Ag and Cs is only of the same order.

On account of these corresponding characteristics the Lilienfeld radiation, produced by metals in the energy range mentioned above, is to be interpreted as the transition radiation due to Ginsburg and Frank. We think it impossible to interpret the Lilienfeld radiation as the visible part of the bremsstrahlung. The Lilienfeld radiation also cannot be interpreted as "plasma radiation" according to the theory of Ferrell,[5] because the plasma radiation only appears on foils with two boundary surfaces, whereas the investigated Lilienfeld radiation is observed on compact metals with only one boundary surface within the depth of penetration of the electrons.

The transition radiation may also contribute to the background of the radiation from thin foils (two boundary surfaces) which had been experimentally studied by Steinmann,[6] and Brown et al.[7]

---

*A detailed publication is intended for the Zeitschrift für Physik.

†This work was supported by the Research Corporation, New York.

[1]W. Ginsburg and I. Frank, J. Exptl. Theoret. Phys. (U.S.S.R.) 16, 15 (1946).

[2]J. E. Lilienfeld, Physik. Z. 20, 280 (1919). J. E. Lilienfeld and F. Rother, Physik. Z. 21, 249 and 360 (1920). F. L. Mohler and C. Boeckner, J. Research Natl. Bur. Standards 6, 673 (1931); 7, 751 (1931); 8, 357 (1932); 9, 413 (1932). P. D. Foote, W. F. Meggers, and R. L. Chenault, J. Opt. Soc. Am. 9, 54 (1924).

[3]F. Rother and W. M. Cohn, Physik. Z. 31, 687 (1931).

[4]K. Sommermeyer, Z. Naturforsch. 4a, 440 (1949).

[5]R. A. Ferrell, Phys. Rev. 111, 1214 (1958).

[6]W. Steinmann, Phys. Rev. Letters 5, 470 (1960).

[7]R. W. Brown, P. Wessel, and E. P. Trounson, Phys. Rev. Letters 5, 472 (1960).

ELECTRONIC EFFECT IN THE ELASTIC CONSTANTS OF GERMANIUM

L. J. Bruner
International Business Machines Watson Laboratory, New York, New York

and

Robert W. Keyes
International Business Machines Research Center, Yorktown Heights, New York

(Received May 25, 1961)

We have measured the elastic constants of pure and heavily doped n-type germanium and discovered a difference which can be attributed to the electronic contribution to the strain energy function. The importance of electronic energy bands in the theory of the elastic constants of metals has been appreciated for a long time. Satisfactory quantitative verification of the electronic theories of elastic constants has not been possible in metals, however, because pertinent parameters of the band structures and their dependence on strain are not known. Such parameters are known for certain semiconductors, however, and, in particular, are far more accurately known for germanium than for any other solid. Therefore germanium provides a unique opportunity for a study of the role of electronic energy in the theory of elastic constants.

We have measured the elastic constants of two samples of germanium. One, "pure," contains less than 10^{14} carriers per cm^3. The other, "heavily doped," contains 3.5×10^{19} arsenic donors per cm^3. The heavily doped sample was a $\frac{3}{4}$-inch cube with exceptionally uniform resistivity, as measured by surface probes.[1] The measurements consisted of the determination of the velocities of 10-Mc/sec ultrasonic waves for an appropriate set of crystal directions by a conventional pulse-echo technique. Measurements were made through the temperature range 4.2°K-240°K. The results at very low temperatures for the pure specimen and the specimen degenerately doped with arsenic are given in Table I. The values of C_{44} as a function of temperature are given in Fig. 1. Our values of C_{44} for the pure specimen differ from those of McSkimin[2] by almost 1% and from those of Fine[3] by 0.5% in the temperature range covered by both sets of measurements.

Referring to Table I, $\frac{1}{3}(C_{11}+2C_{12})$ and $\frac{1}{2}(C_{11}-C_{12})$ are not significantly different in the two specimens, while C_{44} is 5.5% smaller in the heavily doped specimen. Measurements on another specimen of similar doping level but not as homogeneous confirmed this difference in C_{44}. The fact that only C_{44} is affected by the addition of the arsenic characterizes the difference between the samples as an electronic effect. The terms in the strain energy function of the crystal which are proportional to C_{44} involve just those components of strain which alter the conduction band of germanium by removing the degeneracy of the valleys. On the other hand, the terms in the strain energy

Table I. The elastic constants of germanium at 4.2°K (in units of 10^{11} dyne/cm^2).

Specimen	C_{44}	$(C_{11}-C_{12})/2$	$(C_{11}+2C_{12})/3$
Pure	6.80	4.06	7.58
Heavily doped	6.42	4.04	7.66

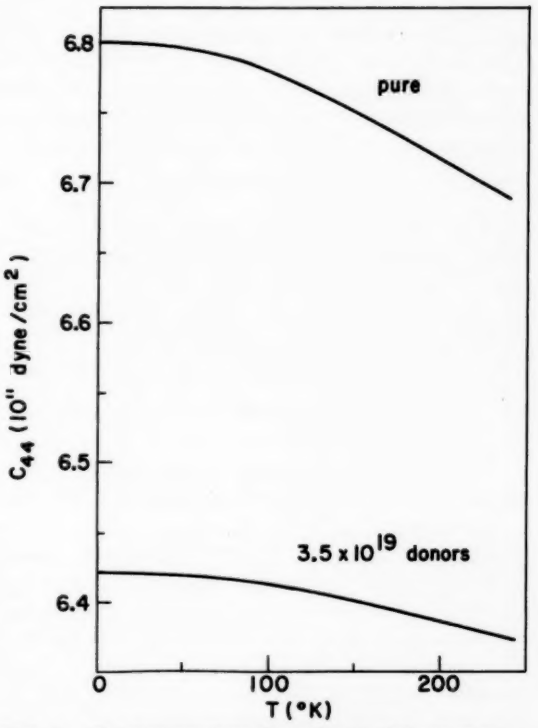

FIG. 1. The temperature dependence of C_{44} in pure and in heavily doped n-type germanium.

function which are proportional to C_{11} and C_{12} contain only components of strain which do not affect the structure of the conduction band of Ge. It can be concluded that the change of elastic constants results from the addition of electrons to the conduction band.

The effect on C_{44} is very large. The addition of 0.08% impurity changes C_{44} by 5.5%, or seventy times the impurity concentration. The large magnitude of the change is also in agreement with the predictions of the electronic interpretation. We have used the usual multivalley-deformation potential model to construct a theory of the electronic contribution to the strain energy function. The theory resembles that of Leigh,[4] who calculated the elastic constants of aluminum from a multivalley-type model, but is not restricted to the degenerate limit assumed by Leigh. According to this model the effect arises in the following way: When the crystal is strained by a pure shear, the energy of some valleys is increased and the energy of other is decreased. The mean energy of the valleys is constant, so that the electronic energy is not changed to first order in the strain. However, in the strained crystal the energy can be lowered by transferring electrons from the higher energy valleys to the lower energy valleys. This re-establishment of statistical equilibrium among the electrons lowers the energy in terms of second order in the strain. Therefore it amounts to a decrease in the shear elastic constant. The quantitative theory shows that in the low-temperature limit,

$$(\delta C_{44}/C_{44})_0 = -(4/3)^{5/3}\pi^{2/3}m^*\Xi_u^2 N^{1/3}/h^2 C_{44}. \quad (1)$$

Here m^* is the density-of-states mass for one valley and the remaining notation is standard. For our heavily doped sample ($N = 3.5\times10^{19}$ cm^{-3}), Eq. (1) gives $(\delta C_{44}/C_{44})_0 = -0.075$. The observed effect is about three-fourths of this.

The highest temperature of our measurements is about one-third of the electronic degeneracy temperature in the doped crystal. The theory predicts that $(\delta C_{44}/C_{44})$ should increase slightly (about 10%) in this range. Figure 1 shows that in fact $(\delta C_{44}/C_{44})$ decreases by about 20%.

Thus the change in elastic constants produced by the solution of arsenic in germanium agrees with an electronic interpretation in two respects: (1) Only C_{44} is changed; (2) the magnitude of the change is very large, and is given semiquantitatively by the theory. The discrepancies with the theory, namely, the difference between the calculated and observed magnitude of $\delta C_{44}/C_{44}$ and the difference between its observed and predicted temperature dependence, probably indicate an inadequacy of the theoretical model. However, it is difficult to completely rule out any effects of inhomogeneities, which are so common in heavily doped germanium. Note that the period of our ultrasonic wave (10^{-7} sec) is very long compared to the scattering times of electrons in germanium so that failure of establishment of equilibrium in the electron populations of the valleys cannot be the source of the discrepancies. For example, the smallest intervalley scattering rate found in all of the samples studied by Weinreich et al.[5] was 5×10^8 sec^{-1} in a high-purity specimen.

We thank Professor S. L. Quimby of Columbia University for permitting us to use certain components of his ultrasonic pulsing equipment.

[1]We are indebted to Dr. G. E. Brock of the IBM Research Center for supervising the preparation of this unusually large and homogeneous specimen of heavily doped germanium.

[2]H. J. McSkimin, J. Appl. Phys. 24, 988 (1953).
[3]M. E. Fine, J. Appl. Phys. 24, 338 (1953).
[4]R. S. Leigh, Phil. Mag. 42, 139 (1951).
[5]G. Weinreich, T. M. Sanders, Jr., and H. G. White, Phys. Rev. 114, 33 (1959).

EVIDENCE FOR THE DOUBLE F MODEL OF THE M CENTER

Bruce J. Faraday, Herbert Rabin, and W. Dale Compton
U. S. Naval Research Laboratory, Washington, D. C.
(Received June 8, 1961)

Recent results of van Doorn[1] on the thermal equilibrium of F and M centers in KCl show that the concentration of M centers varies quadratically with the concentration of F centers. This result supports the proposal of van Doorn and Haven[2] and Pick[3] that the model of the M center is a pair of associated F centers (F_2 model) rather than a vacancy pair plus a single F center as suggested earlier by Seitz[4] and modified by Knox.[5] This Letter presents new results on the relative concentration of F and M centers induced by irradiation, and the implication of these results on the M-center model.

Thin plates of KBr and KCl, approximately 0.09-0.20 mm thick, have been irradiated at liquid helium and liquid nitrogen temperatures with x rays from a 50-kv dc generator for periods up to sixty hours. Sensitive optical absorption measurements show that a weak M band appears with the generation of F centers in KBr, KBr doped with Ca, KCl, and KCl doped with Sr. The data for KBr (Fig. 1) show that the concentration of M centers produced by these low-temperature irradiations is a quadratic function of the F-center concentration. A similar result was found in the KCl specimens. As is shown below, this is evidence that an M center is composed of two F centers. The fact that the divalent impurities and accompanying positive-ion vacancies did not alter the relative concentrations of F and M centers (see Fig. 1) is additional evidence that the positive-ion vacancy is not essential to M-center production.

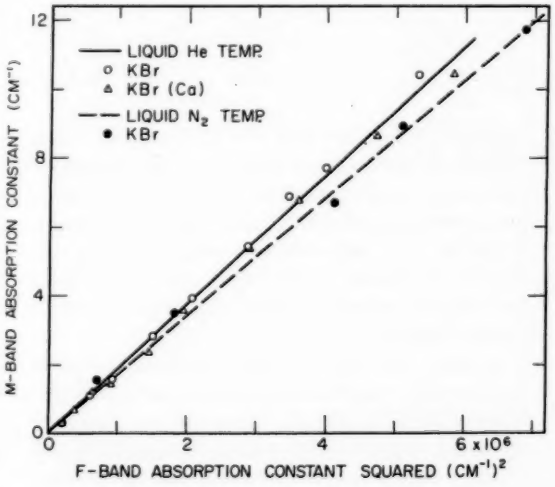

FIG. 1. Absorption constant of the M band vs absorption constant of the F band squared for x-rayed KBr at liquid helium and nitrogen temperatures. The optical measurements were taken at the irradiation temperature.

The x-ray production of M centers is predictable from the probability of forming two F centers as neighbors. If it is assumed all F centers are produced with equal likelihood, the probability that two F centers will be formed as neighbors is proportional to $(n_F/N)^2$, where n_F is the concentration of F centers and N is the concentration of negative-ion sites in the normal lattice. Thus the concentration of M centers is given by

$$n_M = K n_F^2/N, \tag{1}$$

where K is a constant. Figure 1 shows this predicted quadratic dependence. Using the Gaussian form of Smakula's formula[6] for both F and M centers, it follows that

$$\left(\frac{\alpha_M}{\alpha_F^2}\right)\left(\frac{W_M}{W_F^2}\right)\left(\frac{f_F^2}{f_M}\right) = 0.87\times 10^{17}\left(\frac{K}{N}\right)\left(\frac{C_F^2}{C_M}\right), \tag{2}$$

where $C=\mu/(\mu^2+2)^2$, μ being the index of refraction, α = absorption constant in cm^{-1}, W = the absorption half-width in ev, and f = the oscillator strength. The indices F and M refer to the F and M centers, respectively. Table I gives a tabulation of the half-widths and values of α_M/α_F^2 obtained from a least-squares fit of the data of Fig. 1. Assuming that negligible diffusion of F centers occurs at liquid helium and nitrogen temperatures, M centers can only be formed during x raying when two F centers are formed as nearest neighbors. In this case $K=12$, corresponding to the number of nearest negative-ion sites surrounding an F center. Average values of f_F are taken from the literature.[7,8] The values of f_M so calculated (0.12 to 0.20, Table I) appear quite reasonable in view of the simplicity of the calculation.[9]

In light of the low-temperature results, two examples of M-center formation at higher temperatures can be considered. First, the M-center concentration in KBr and KCl crystals x-rayed at

Table I. Data for calculating f_M for KBr and KCl assuming $K = 12$.

	α_M/α_F^2 (cm)	W_M/W_F (ev/ev)	f_F/f_M [a]	f_M
KBr (He temp.)	1.87×10^{-6}	0.052/0.158	3.2	0.15
KBr (N_2 temp.)	1.71×10^{-6}	0.063/0.190	4.0	0.12
KCl (He temp.)	1.95×10^{-6}	0.056/0.169	2.7	0.20
KCl (N_2 temp.)	1.96×10^{-6}	0.066/0.194	2.9	0.18

[a] Average values of f_F are taken from the literature for a Gaussian F band: $\langle f_F\rangle_{av}(\text{KBr}) = 0.48$,[7] and $\langle f_F\rangle_{av}(\text{KCl}) = 0.53$.[8]

liquid helium or nitrogen temperatures increased by a factor of about fifty upon warming to room temperature.[10] This suggests that F centers some distance apart aggregate to form M centers during warmup. Second, F- and M-center equilibrium after room-temperature x raying may be studied. The published data of Mador et al.[11] for NaCl and LiF are particularly appropriate for this purpose since optical absorption measurements were made transversely to the x-ray direction, insuring uniform coloration along the optical path. A treatment of their data to test the quadratic relation between α_M and α_F is shown in Fig. 2. It is again seen that α_M is a linear function of α_F^2. Equation (2) can now be used to compute a value of K for NaCl and LiF at room temperature, assuming a value of the oscillator strengths.[12] K may now be interpreted as follows. If two F centers are contained in a spherical volume of K negative-ion sites, they associate to form an M center. If a is the lattice constant, i.e., the distance between like ions along a $\langle 100\rangle$ direction, then a "sphere of interaction" for F centers of radius r is given approximately by the relation $(4\pi/3)r^3 \simeq Ka^3/4$. It follows that $r/a \simeq 0.39(K)^{1/3}$, which is the maximum number of lattice constants over which F centers join to form M centers. Using values of K calculated from Eq. (2) from the least-squares slopes of Fig. 2, r/a can thus be determined. Values of K and r/a are as follows:

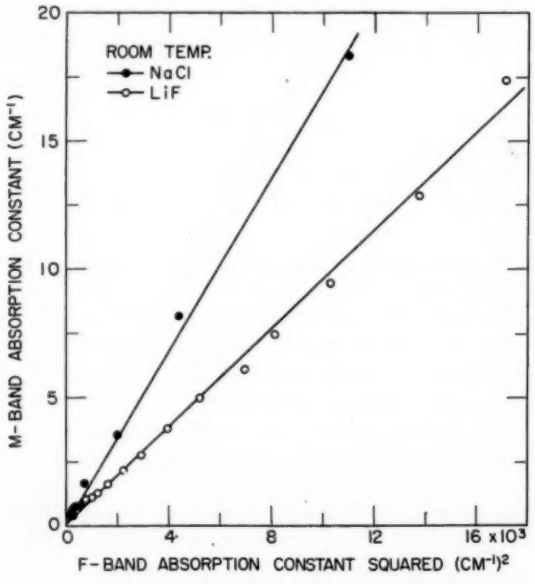

FIG. 2. Absorption constant of the M band vs absorption constant of the F band squared for NaCl and LiF x-rayed and measured at room temperature, taken from Mador et al.[11]

	K	r/a
NaCl	7000	7.4
LiF	4400	6.4

This result implies that the interaction of two F centers is sufficiently great at room temperature that two F centers separated by six or seven lattice constants join to form M centers. The nature of the mechanism which promotes such an association is not understood. Alternatively this might be taken as evidence for a nonrandom distribution of F centers.

A value of K for KCl can also be determined for van Doorn's high-temperature data[1] (~1000°K). This value is roughly a factor of ten lower than the room-temperature values, suggesting an equilibrium between the formation and the breakup of M centers at the high temperature.

A substantial amount of evidence now appears to support the F_2 model of the M center. It has been demonstrated that F and M centers are quadratically related in cases of both thermal quench-

ing and x raying over a wide temperature and concentration range in a variety of alkali halides. Furthermore, this model is in accord with the requirement of inversion symmetry,[13] the absence of dielectric loss[14] and magnetic susceptibility,[15] and the inconclusiveness of electron spin resonance[16] of the M center.

In light of the above discussion the suggestion of Pick[3] that the R and N centers are higher aggregates of F centers has been examined. Treating unpublished data[17] for NaCl that had been uniformly irradiated with gamma rays at room temperature, it was found that the R_2-center absorption varied approximately as the 1.5 power of the M-center absorption. This supports the contention that the R center is an aggregate of an M and F center, or simply three F centers as suggested by Pick. A more extensive study is indicated.

The authors are indebted to Dr. C. C. Klick for many helpful discussions.

[1]C. Z. van Doorn, Phys. Rev. Letters 4, 236 (1960).
[2]C. Z. van Doorn and Y. Haven, Philips Research Repts. 11, 479 (1956), and C. Z. van Doorn, Philips Research Repts. 12, 309 (1957).
[3]H. Pick, Z. Physik 159, 69 (1960).
[4]F. Seitz, Revs. Modern Phys. 18, 384 (1946).
[5]R. S. Knox, Phys. Rev. Letters 2, 87 (1959).
[6]D. L. Dexter, Phys. Rev. 101, 48 (1956), Eq. (27).
[7]See, for example, C. J. Rauch and C. V. Heer, Phys. Rev. 105, 914 (1957), and F. Lüty, Z. Physik 160, 1 (1960).
[8]In addition to reference 7 see F. G. Kleinschrod, Ann. Physik 27, 97 (1936), and R. H. Silsbee, Phys. Rev. 103, 1675 (1956). Also a treatment by Seitz[4] of data from H. Pick, Ann. Physik 31, 365 (1938).
[9]Although there appears to be good agreement with Okura's value of f_F/f_M of 2.4 determined from F-center bleaching of KCl, a linear rather than quadratic relation between F and M centers was assumed; see H. Okura, J. Phys. Soc. Japan 12, 1313 (1957). In the case of two F centers per M center Okura's value is reduced to 1.2, a factor of about two to three lower than those given in Table I. It is quite possible that the bleaching technique ignores the formation of other centers, like the A center; see, for example, M. Hirai, J. Phys. Soc. Japan 14, 1400 (1959).
[10]It should be pointed out that this technique provides a method of obtaining comparatively large M-center concentrations.
[11]I. L. Mador, R. F. Wallis, M. C. Williams, and R. C. Herman, Phys. Rev. 96, 617 (1954), Figs. 7 and 9.
[12]The value of f_F^2/f_M is taken to be 1.61 using the average of the data for KBr and KCl from Table I.
[13]A. W. Overhauser and H. Rüchardt, Phys. Rev. 112, 722 (1958).
[14]G. Jacobs, J. Chem. Phys. 27, 217 (1957).
[15]E. Sonder, Bull. Am. Phys. Soc. 6, 114 (1961).
[16]W. C. Holton, H. Blum, and C. P. Slichter, Phys. Rev. Letters 5, 197 (1960).
[17]Obtained in connection with an earlier study, W. D. Compton, Phys. Rev. 107, 1271 (1957).

SIZE-DEPENDENT RELAXATION TIMES AT LIQUID HELIUM TEMPERATURES*

F. R. Nash

Columbia Radiation Laboratory, Columbia University, New York, New York

(Received June 26, 1961)

Recovery times have been observed in one of the copper Tutton salts which depend upon the size of the crystal(s) employed.[1] The salt in question is fully concentrated $Cu(NH_4)_2(SO_4)_2 \cdot 6H_2O$. The paramagnetic ion is Cu^{+2} ($S=\frac{1}{2}$) and the two ions per unit cell give rise to two lines.[2] However, at high concentrations the two lines coalesce to form one broad line whose full width at half maximum varies from 170 to 450 oersteds depending upon the angle between the crystal axis and the magnetic field.

The relaxation times were measured with an X-band pulse-decay superheterodyne spectrometer, the output of which was the dynamic recovery curve of the spin system.[3] The relaxation times were determined from the exponential tails of the decays, in the region where the spin temperature ≈ lattice temperature.

The crystals reported on were prepared in two different ways. In the first instance a fine powder of crystallites was allowed to grow slowly over a period of 24 hours. The second method involved the preparation of a supersaturated solution by heating. The solution was stirred continually as it cooled to room temperature with the result that a fine powder of tiny crystals was deposited in the bottom of the beaker. In both cases the crystals were then dried by exposure to air and carefully sorted according to size using a series of sieves. The hole sizes in the ten sieves ranged from 37 to 1000 microns. Only naturally grown single crystals were used

VOLUME 7, NUMBER 2 PHYSICAL REVIEW LETTERS JULY 15, 1961

in these experiments although some single crystals were crushed and tested to see that the size effect was qualitatively unaltered.

The cavity was entirely filled with Styrofoam except for a pocket ≈ 10 mm^3 which was located in the region of the cavity where $H_{rf} \approx 0$. This placement was to allow the use of an appreciable volume of sample and still keep the cavity loading $\leq 10\%$.[3]

The results are presented in Figs. 1 and 2. It seems reasonable to suggest that crystals which are grown quickly (≈ 1 minute) are sufficiently strained so that some internal energy conversion mechanism alleviates the apparent bottleneck. One might suggest phonon-phonon interactions but the observed temperature dependence is not as strong as this mechanism would imply.

Within the experimental error of $\approx \pm 10\%$ one can see that $\tau_{1/e} \propto L$, where L is some characteristic length of any one of the many crystallites in a given portion of sample.

From measurements made on single crystals whose smallest dimensions were ≈ 1-2 mm, it was noted that the transition from the region where $\tau_{1/e} \propto L$ to the region where $\tau_{1/e}$ is independent of L occurs for $L \approx 1$ mm. Furthermore, the relaxation times of the single crystals were $\approx 20\%$ shorter than those times in the sample where $L \approx 855$ microns. Presumably this is related to the fact that large single crystals are somewhat more strained than smaller ones. The same kind of bottleneck has been seen in the deuterated crystals of the same species and concentration and also in 30% concentration hydrated crystals.

In order to test that the liquid helium in contact with the sample was really cooling the individual particles, a very light smear of the $L < 37$ microns sample was made on the surface of the Styrofoam cavity insert in the region of $(H_{rf})_{max}$. This was to assure the helium liquid clear access to all the grains in the sample. Exactly the same results were obtained as when the sample consisted of 10 mm^3 of tightly packed powder, in the weak-field region of the cavity.

Spatial spin diffusion as the explanation for this size effect can be ruled out on the basis of an order-of-magnitude calculation of the overall diffusion time as well as dependence upon length and lattice temperature.[4] The theories of phonon imprisonment in paramagnetic crystals[5] would indicate that lattice-bath relaxation times are being observed.[6] Indeed, there is fairly good agreement between the theory[5] and the observed results. To see that phonon trapping is reasonable one can make an order-of-magnitude estimate of the phonon mean free path (m.f.p.) in the central region of the spin

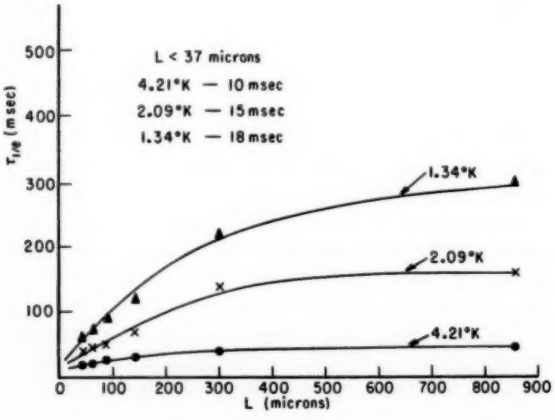

FIG. 1. Relaxation times in quickly grown crystals of 100% $Cu(NH_4)_2(SO_4)_2 \cdot 6H_2O$ vs characteristic length of crystal.

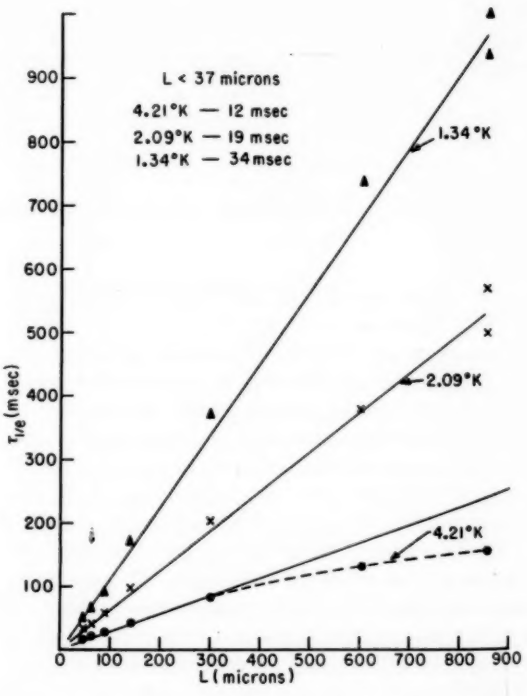

FIG. 2. Relaxation times in slowly grown crystals of 100% $Cu(NH_4)_2(SO_4)_2 \cdot 6H_2O$ vs characteristic length of crystal.

resonance:

$$\text{m.f.p.} \approx \langle n \rangle_{\text{av}} v\rho(\nu)\Delta\nu T_1/\Delta N$$
$$\approx (kT/h\nu)^2 24\pi\nu^2\Delta\nu T_1/v^2 N,$$

where $\langle n \rangle_{\text{av}}$ = number of phonons per mode $\approx kT/h\nu$, v is the mean acoustic velocity, $\rho(\nu)$ is the density of lattice modes $= 12\pi\nu^2/v^3$, $\Delta\nu$ is the full width of the spin resonance, T_1 is the spin-lattice relaxation time, and $\Delta N = NkT/2h\nu$. If $T = 1.34°\text{K}$, $\nu = 9.6\times10^9$ cps, $T_1 = 10^{-2}$ sec, $v = 2.5\times10^5$ cm/sec, and $N = 3\times10^{21}$ spins/cm^3, then m.f.p. ≈ 30 microns or 3×10^{-3} cm.

There are, however, two aspects of this effect which are not clear.

(1) Tests were made on a fully concentrated single crystal in which the sample was cooled by helium gas (pressure ≈ 1 mm of Hg) at 4.21°K, 2.09°K, and 1.34°K. The run was repeated but this time the crystal was cooled directly by liquid helium. Within experimental error the relaxation times in both cases were the same. The test was performed on another single crystal of a different shape and again it did not matter whether the crystal was cooled by helium liquid or gas.

(2) Phonon trapping theoretically[5] depends upon a direct spin-lattice interaction. In addition, experiments which have been performed by the author at lower concentrations indicate that the spin-lattice relaxation time is concentration dependent. However, the theoretical calculations[7] which have been carried out for the concentration-dependent, first order spin-lattice interactions are inadequate to explain the shortness of the spin-lattice relaxation times obtained by extrapolating the present data to $L \approx 0$.

The author would like to acknowledge his indebtedness to Professor C. H. Townes and to Dr. J. A. Giordmaine for their innumerable suggestions, their time, and their encouragement.

Thanks are also due to Professor H. Boorse and H. Louie for liquid helium and to B. Biavati and S. Zemon for discussions concerning low-temperature techniques.

---

*Work supported jointly by the U. S. Army Signal Corps, the Office of Naval Research, and the Air Force Office of Scientific Research.

[1]For the observation of apparent size effects by using the magnetic susceptibility of paramagnetic crystals at audio frequencies, see, e.g., C. J. Gorter, L. C. Van der Marel, and B. Bolger, Physica 21, 103 (1955), or L. C. Van der Marel, J. Van der Broek, and C. J. Gorter, Physica 23, 361 (1957).

[2]B. Bleaney, R. P. Penrose, and B. I. Plumpton, Proc. Roy. Soc. (London) A198, 406 (1949).

[3]K. D. Bowers and W. B. Mims, Phys. Rev. 115, 285 (1959).

[4]N. Bloembergen, Physica 15, 386 (1949); H. Fröhlich and W. Heitler, Proc. Roy. Soc. (London) A155, 640 (1936).

[5]J. A. Giordmaine and C. H. Townes (unpublished).

[6]J. H. Van Vleck, Phys. Rev. 59, 724 (1941); J. A. Giordmaine, L. E. Alsop, F. R. Nash, and C. H. Townes, Phys. Rev. 109, 302 (1958); P. W. Anderson, Phys. Rev. 114, 1002 (1959).

[7]I. Waller, Z. Physik 79, 370 (1932); S. A. Al'tshuler, Bull. Acad. Sci. U.S.S.R. 20, 1098 (1956).

OSCILLATORY PHOTOCONDUCTIVITY IN InSb†

W. Engeler,* H. Levinstein, and C. Stannard, Jr.
Syracuse University, Syracuse, New York
(Received June 21, 1961)

The addition of Cu to InSb has been shown by Blunt[1] to produce two deep acceptor levels. He also observed a series of oscillations in the extrinsic photoconductive response associated with the lower of these two levels. To investigate the mechanism responsible for this behavior the properties of impurities similar to Cu were examined. Ag and Au, which had also been found to produce two deep acceptor levels,[2] were examined in addition to Cu and Ni.

Oscillatory behavior of the photoconductive response at liquid He temperature was observed for all of these impurities as shown in Fig. 1. In all cases the oscillations observed have minima separated by constant energy intervals. The locations of these minima depend on the impurity and are thus distinct from lattice absorptions at 27.5 and 33.5 μ which are independent of impurity. Figure 2 shows a plot of the number of the minimum vs the energy at which it occurs, for all of the impurities investigated. A straight line is obtained for each impurity. The slopes of these lines, corresponding to the energy difference between successive minima as calculated by a least-squares fit of the data, are identical within experimental error. In the case of gold it was possible to obtain the value of the long-wavelength threshold of the photoconductive response. The intercept of the straight line with the energy axis yields an energy value in agreement with the threshold wavelength. This value is indicated by the arrow in Fig. 1. Since the threshold of the Cu and Ag response curves was not within the range of the optical equipment available, the assignment of the number of the minima was based on the estimate of the position of threshold energy by Hall measurements. The fourth curve shown in Fig. 1 was obtained from a sample which was originally prepared to contain Ni. The photoconductive response cutoff of this sample shows a wide departure from the energy of the Ni level as determined by the Hall data. It is highly probable therefore that the response is due to an unknown impurity which was introduced into the sample during its processing. Since the maximum solubility of Ni in InSb is of the order of 10^{14} atoms/cc, only a small additional impurity would be necessary to cause such an effect. The values of slopes

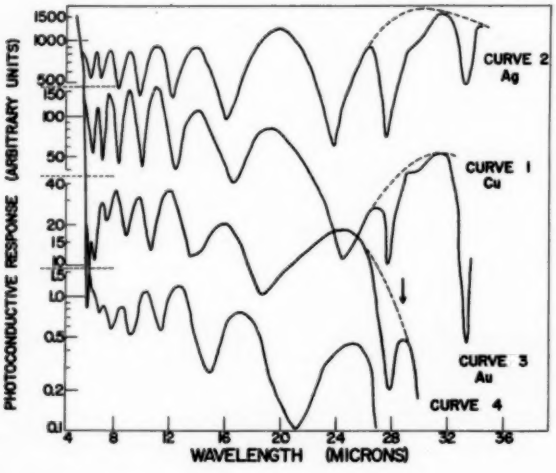

FIG. 1. Extrinsic photoresponse of InSb.

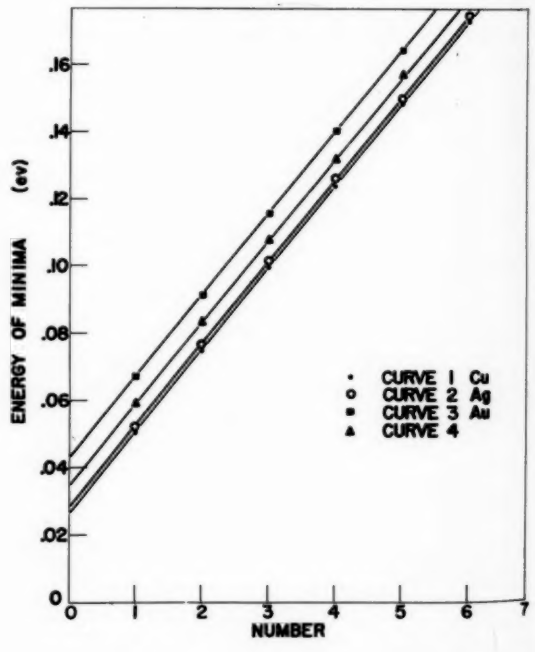

FIG. 2. Spectral response minima for various impurities in InSb.

Table I. Summary of results.

Curve	Impurity	Slope (ev)[a]	Intercept (ev)	Activation energy (ev) (from Hall measurements)
1	Cu	0.0244	0.026	0.023
2	Ag	0.0244	0.028	0.023
3	Au	0.0244	0.043	0.032
4	...	0.0244	0.035	...

[a]Error does not exceed 0.0001.

and intercepts together with Hall data for the various impurities are summarized in Table I.

These data strongly suggest that the observed spectral response is composed of a series of superimposed spectral curves. The long-wavelength threshold corresponds to the excitation of a hole from the impurity state to the valence band. The next threshold corresponds to the same process accompanied by the emission of a longitudinal optical phonon, succeeding thresholds at shorter wavelengths to the emission of 2, 3, 4, etc., phonons, respectively.

The slopes of the curves in Fig. 2 are then the energy of the longitudinal optical phonon. The value obtained in this manner is in good agreement with the value of 0.024 ev obtained by Hall, Racette, and Ehrenreich[3] from tunnelling experiments and the value of 0.0244 ev recently reported by Fray, Johnson, and Jones.[4]

A process of this type can be explained as follows. Starting from the threshold at $k = 0$ and going to higher energy, the transition probability for direct transitions to the impurity level first increases with the increase in the density of states of the valence band. This is followed by a decrease of this transition probability for larger k values due to the decrease in the density of states of the impurity level. This decrease is slowed by the possibility of indirect transitions. When a photon energy is reached where a longitudinal optical phonon can be emitted, the transitions can again take place at $k = 0$ and the process is repeated with the emission of this phonon. The optical absorption constant is directly related to this transition probability. The magnitude of the spectral response in turn depends on the relative magnitude of this absorption and other competitive absorption processes. Because of the lack of knowledge of the competitive processes, the magnitude of the observed oscillations cannot be directly related to the transition probabilities. This behavior should be observable in other polar compounds and should be a valuable tool in the study of these materials.

The authors acknowledge the assistance of L. Apker, H. Ehrenreich, and W. W. Tyler of the General Electric Research Laboratory in the interpretation of these results.

---

†Sponsored by Air Research and Development Command, U. S. Air Force.

*Now at General Electric Research Laboratory, Schenectady, New York.

[1]R. F. Blunt, Bull. Am. Phys. Soc. 3, 115 (1958).

[2]W. Engeler and H. Levinstein, Bull. Am. Phys. Soc. 6, 156 (1961).

[3]R. N. Hall, J. H. Racette, and H. Ehrenreich, Phys. Rev. Letters 4, 456 (1960).

[4]S. J. Fray, F. A. Johnson, and R. H. Jones, Proc. Phys. Soc. (London) 76, 939 (1960).

AUTO-IONIZATION OF THE $(1s2s2p)\ ^4P_{5/2}$ LEVEL IN Li AND He^-

Jerry L. Pietenpol*

Columbia University, New York, New York

(Received June 20, 1961)

The negative helium ion has been observed experimentally,[1-3] and Sweetman[4] has obtained a lower bound of 10^{-5} second for its lifetime. Arguments have been advanced[5,6] indicating that the observed metastable state is a $(1s2s2p)\ ^4P_{5/2}$ configuration. The purpose of this note is to report a theoretical estimate of the lifetime of the state for auto-ionization. The calculation has been made both for negative helium and for lithium; the result is of interest in the latter case because of the possibility of measuring the fine and hyperfine structure of the level.

The state is radiatively metastable because of the spin selection rule. Holøien and Midtdal[5] have shown by an elaborate variational calculation that this level in He^- lies below the $1s2s$ level of the helium atom, and have pointed out that the state is therefore not subject to auto-ionization in the usual way. The only available final state consistent with angular-momentum and parity conservation is then $(1s^2kf)\ ^2F_{5/2}$. The Coulomb, spin-orbit, and spin-other-orbit operators have vanishing matrix elements for the transition, but the process can proceed by the magnetic spin-spin interaction between two electrons.

If we write the spin-spin operator in the form

$$H' = -\mu_0{}^2(\vec{\sigma}_1\cdot\nabla_1)(\vec{\sigma}_2\cdot\nabla_1)(1/r_{12}),$$

the matrix element can be evaluated by a double partial integration. (It is necessary to exclude an infinitesimal sphere about the point of singularity, so that one must look for surface terms here. These terms vanish, however, for any matrix element between states of different spin.) We used antisymmetrized product wave functions, with screened hydrogenic functions for the bound electrons and a plane wave for the continuum. The effective Z's and the energy of the initial state were obtained from a variational calculation, including exchange between $2s$ and $2p$. The parameters are as follows:

For Li: initial-state $Z_{1s}=3.0$, $Z_{2s}=2.0$, $Z_{2p}=1.7$, final-state $Z_{1s}=2.69$, kinetic energy of continuum electron $E=3.95$ rydbergs.

For He^-: initial-state $Z_{1s}=2.0$, $Z_{2s}=1.0$, $Z_{2p}=0.67$, final-state $Z_{1s}=1.69$, $E=1.45$ rydbergs.

The integrations were carried out analytically. The result for the lifetime of the state is 1.6×10^{-5} sec for Li, and 1.7×10^{-3} sec for He^-. Variation of the Z parameters within reasonable limits produces a change of no more than a factor of two in the lifetime. In the very simple approximate wave functions employed, the use of a plane wave for the continuum state is justified for helium (since the centrifugal barrier effectively prevents the electron from penetrating the $1s^2$ core), but is questionable for lithium. The initial-state wave function did not include correlation between the $2s$ and $2p$ electrons; this effect would be expected to lengthen the calculated lifetimes.

The author is indebted to Professor H. M. Foley and Professor R. Novick for valuable discussions, and to Professor N. M. Kroll for suggesting the spin-spin interaction as the mechanism of the process.

---

*Quincy Ward Boese Predoctoral Fellow.

[1]J. W. Hiby, Ann. Physik 34, 473 (1939).

[2]V. M. Dukel'skii, V. V. Afrosimov, and N. V. Fedorenko, J. Exptl. Theoret. Phys. (U.S.S.R.) 30, 792 (1956) [translation: Soviet Phys.-JETP 3, 764 (1956)].

[3]P. M. Windham, P. J. Joseph, and J. A. Weinman, Phys. Rev. 109, 1193 (1958).

[4]D. R. Sweetman, Proc. Phys. Soc. (London) 76, 998 (1960).

[5]E. Holøien and J. Midtdal, Proc. Phys. Soc. (London) A68, 815 (1955).

[6]Ta-You Wu, Phil. Mag. 22, 837 (1936).

STRUCTURE IN THE KINETIC ENERGY SPECTRUM OF FRAGMENTS FROM THERMAL-NEUTRON-INDUCED FISSION OF U^{235}†

W. M. Gibson
Bell Telephone Laboratories, Murray Hill, New Jersey

and

T. D. Thomas and G. L. Miller
Brookhaven National Laboratory, Upton, New York
(Received June 19, 1961)

We have observed fine structure in the kinetic energy spectra of the heavy fragments from thermal-neutron-induced fission of U^{235}. This fine structure in the energy spectra is reflected as fine structure in the calculated fission-mass-yield distribution.

A target of 5 $\mu g/cm^2$ of U^{235} evaporated onto a 15-$\mu g/cm^2$ backing of VYNS film was placed between two 1.5-cm^2 p-n junction semiconductor particle detectors 5 cm apart. The target, counters, and integrating preamplifiers were enclosed in an evacuated aluminum can, which was lowered into the thermal column of the Brookhaven graphite research reactor. The pulses from the preamplifiers were further amplified by linear amplifiers whose outputs were fed into a coincidence circuit and into the two axes of a 64×64 two-dimensional pulse-height analyzer.[1] The pulse-height analyzer was triggered by the coincidence circuit and, therefore, recorded only those events in which a fission fragment entered each counter within the resolving time of the coincidence circuit (~ 0.1 μsec).

Two separate experiments were performed. In the first experiment, counters made by diffusion of phosphorus into 100-ohm-cm p-type silicon were used at a reverse bias of 100 volts. The coincidence counting rate was 2400 fissions/minute, and a total of 1.66×10^6 fissions was recorded. In the second experiment, the counters were of 300-ohm-cm silicon biased at 100 volts. Because there was evidence for a small low-energy tail on the kinetic energy spectra in the first experiment, two Plexiglas collimators were used in the second to keep the fission fragments from hitting the edges of the counters. The coincidence counting rate was 500 fissions/minute with a total of 6.1×10^5 fissions. Summation of the mass spectra over the total kinetic energy range of 70 Mev to 250 Mev gave a peak-to-valley ratio of 370/1.

Figure 1 shows the very pronounced structure in the energy spectra of heavy fragments in coincidence with light fragments of greater than 100 Mev. The energy channels are about 1 Mev wide in both directions. Stein's time-of-flight data have been used to calibrate the energy scale.[2] Recent time-of-flight measurements on thermal-neutron fission of U^{235} by Milton[3] show essentially the same structure. We observed no structure in the spectra of the light fragments nor in the spectra of heavy fragments in coincidence with light fragments of less than about 100 Mev.

The fission yield and average total kinetic energy as a function of mass number calculated from the

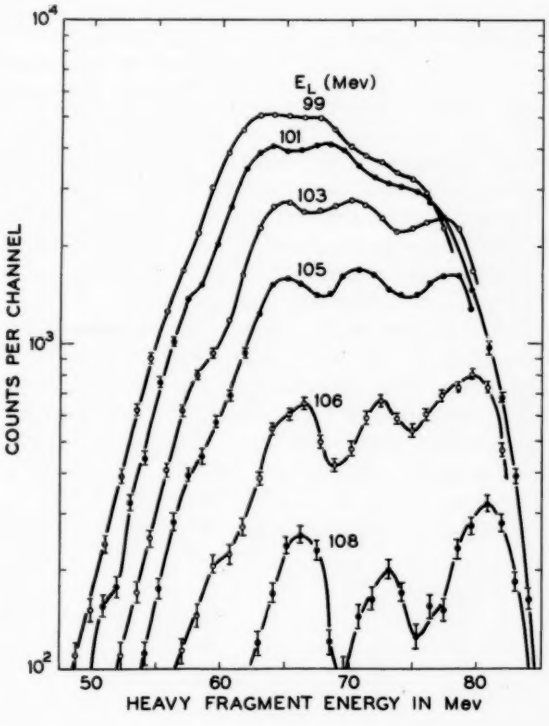

FIG. 1. Spectra of heavy fission fragments in coincidence with given light fragment energies, E_L. The open points and broken curves correspond to a heavy fragment into counter A and a light fragment into counter B; the closed points and unbroken curves to the reverse.

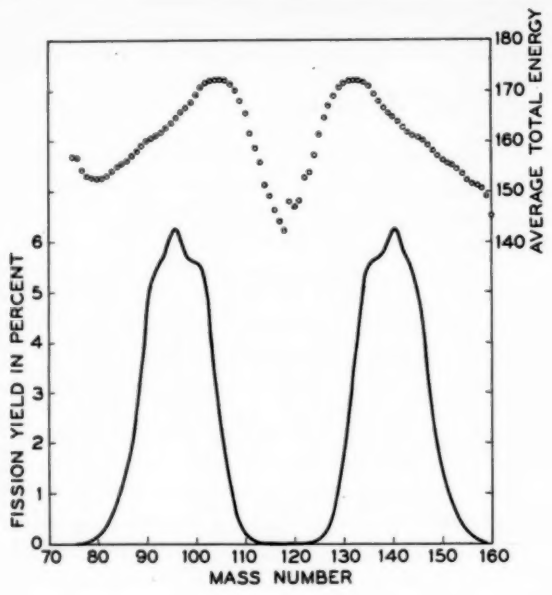

FIG. 2. Fission yield and average total kinetic energy as a function of mass number.

experimental data are shown in Fig. 2. Except in the regions of mass 100 and mass 134, the mass-yield data are in good agreement with the data obtained by Milton, who used the time-of-flight technique.[4] The kinetic energy curve falls somewhat lower than does Milton's, the difference being due to a difference between the time-of-flight measurements of Milton and those of Stein.[2]

The two shoulders on the mass-yield curve occur at light fragment masses of 92 and 101 and the peak occurs at light mass 96; the maxima in the curves of Fig. 1 correspond to light fragment masses of 91, 96, and 101. Thus, the structure in the mass-yield curve appears to be related to the structure in the kinetic energy spectrum. Mass-yield curves for specific values of the total kinetic energy differ from the summed curve of Fig. 2 in that they are narrower and in general do not show the fine structure apparent in Fig. 2. The structure in the total mass distribution arises from the fact that the mass-yield curves for different total kinetic energy tend to fall into three groups. For total kinetic energies less than 162 Mev, the most probable light fragment mass number is about 92; for energies between 164 and 171 Mev, about 96; and for energies greater than 173 Mev, about 101.

The highest energy peaks in the curves shown in Fig. 1 occur at energies corresponding to a heavy mass of about 135, which may be associated with the closed shells of 82 neutrons and 50 protons. However, there is no obvious correlation between closed shells and the other two peaks which correspond to heavy fragment masses of about 140 and 145 (or light masses of 96 and 91).

We have conducted similar measurements on the spontaneous fission of Cf^{252}. An experiment in which 6×10^5 fissions were recorded showed that any fine structure that may exist in the kinetic energy spectrum of Cf^{252} is much less pronounced than in the thermal neutron fission of U^{235}.

We are pleased to acknowledge the assistance of C. A. Boulin, who constructed the preamplifiers, and T. C. Madden, who made the counters and helped design the apparatus.

---

†Research was performed in part under the auspices of the U. S. Atomic Energy Commission.

[1]R. L. Chase, Brookhaven National Laboratory Report BNL-3838, 1958 (unpublished).

[2]W. E. Stein, Phys. Rev. 108, 94 (1957).

[3]J. C. D. Milton and J. S. Fraser, following Letter [Phys. Rev. Letters 7, 67 (1961)].

[4]J. C. D. Milton, quoted by G. C. Hanna, Proceedings of the International Conference on Nuclear Structure, Kingston, Canada, edited by D. A. Bromley and E. W. Vogt (University of Toronto Press, Toronto, 1960), p. 866.

PROMPT FISSION YIELDS AND TOTAL KINETIC ENERGY BEHAVIOR FROM TIME-OF-FLIGHT MEASUREMENTS

J. C. D. Milton*
Lawrence Radiation Laboratory, Berkeley, California
and
J. S. Fraser
Chalk River Laboratories, Atomic Energy of Canada Limited, Chalk River, Ontario, Canada
(Received June 19, 1961)

An improved version of the time-of-flight apparatus described previously[1,2] has been used to study the thermal neutron fission of U^{233}, U^{235}, and Pu^{239} using a neutron beam of intensity about 10^9 neutrons sec^{-1} cm^{-2} from the NRU reactor. The sources, ranging from 20 to 40 μg cm^{-2}, were electrosprayed onto two cross-laminated VYNS films of total surface density 7 μg cm^{-2} which had been previously coated with 18 μg cm^{-2} of gold to make them electrically conducting. The energy loss caused by source and backing thickness was measured for the actual sources used in the experiment and found to be 1.1 ± 0.3 Mev in good agreement with the value calculated from the known thicknesses.

The fragments were detected at the end of their nearly equal 178-cm flight paths by 4-inch diameter secondary electron detectors which gave the apparatus a resolving time (FWHM) of 2.5 nanoseconds. The mass resolution including the contribution of timing jitter, recoil from neutrons, and source thickness was calculated to be 2 mass units.

In all, well over 10^6 events were processed on $U^{235}+n$ (including some with the unequal flight paths of 270-180 cm) but the most carefully controlled series consisted of 1.48×10^5, 1.55×10^5, and 1.03×10^5 events for U^{233}, U^{235}, and Pu^{239}, respectively, and it is on this set that the data presented here are based. The experimental results on Cf^{252} are not new but are those of reference 1.

An experiment of this type conveys an enormous amount of information. The purpose of this Let-

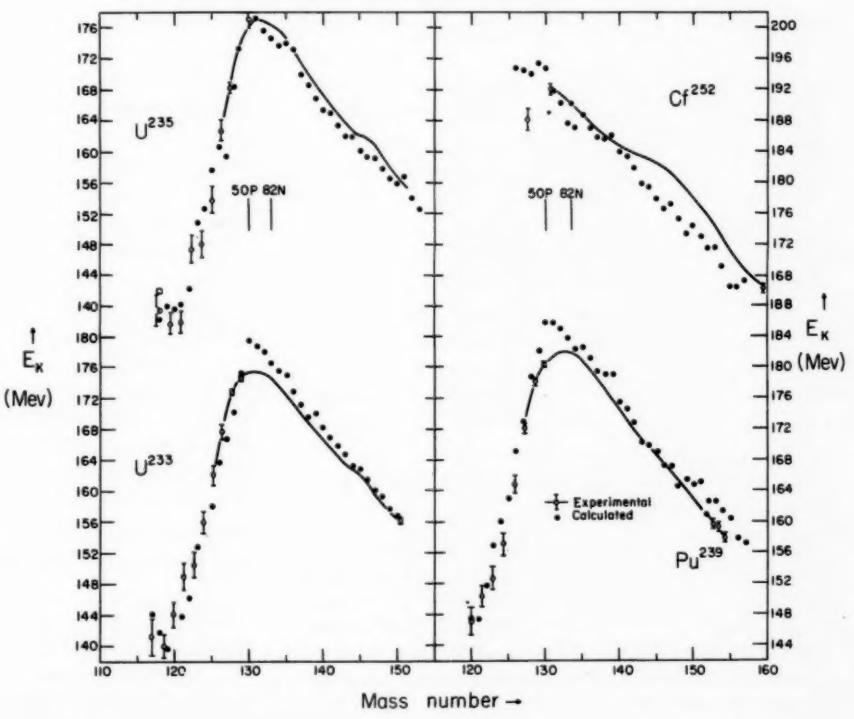

FIG. 1. The average total kinetic energy as a function of the mass of the heavy fragment. In the mass region 130-150 the experimental curve is determined by over 20 points, each with a statistical error of less than 0.25 Mev.

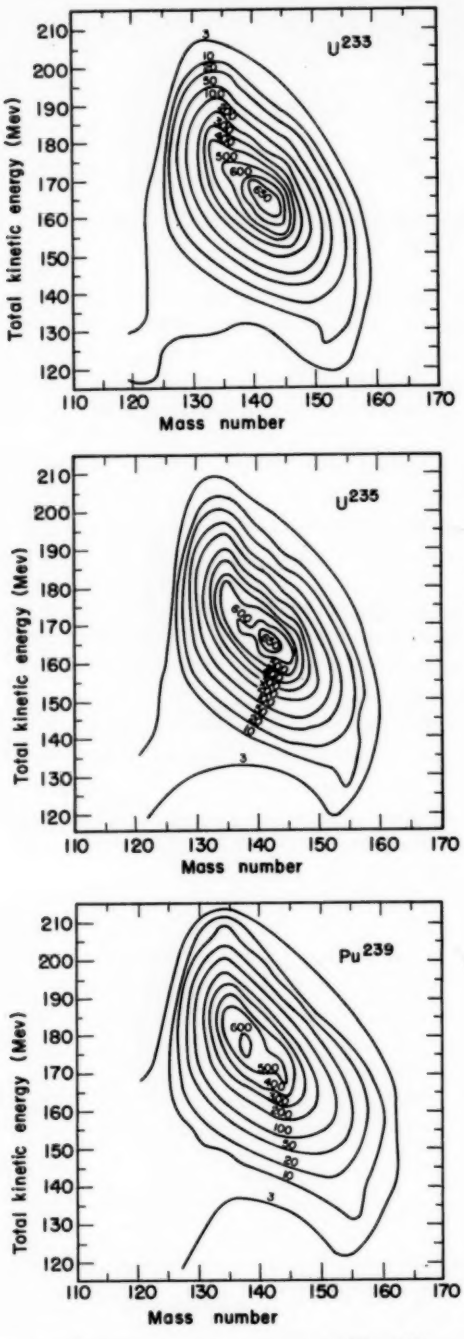

FIG. 2. Mass-energy contours for U^{233}, U^{235}, and Pu^{239}. The numbers attached to the contours are events $(10^5 \text{ fissions})^{-1}$ (mass unit)$^{-1}$ (2.5 Mev)$^{-1}$. Some idea of the statistical accuracy may be gained from the fact that the number of events in each cell of the matrix from which the contour diagram was made is approximately 2½ times the contour label.

ter is to note 3 points: (1) There is a dramatic drop in the total kinetic energy near symmetry; (2) there is a clearly marked fine structure in the mass yield which is most prominent at high total kinetic energies; and (3) a possible explanation for the phenomenon (1).

The behavior of the kinetic energy is illustrated in Fig. 1. Except in the case of Cf^{252}, there is a drop in kinetic energy of 30-40 Mev in approaching symmetric mass division. At first it seemed impossible to account for this dip in terms of the balance of energy between the mass energy release E_R, and the excitation energy made up of components E_B (neutron binding), E_{nk} (neutron kinetic), and E_γ (gamma rays), but this turned out to be incorrect. The solid points in Fig. 1 are calculated from the formula $E_K = \max\langle E_R\rangle - \nu(\langle E_B\rangle + E_{nk}) - E_\gamma$. The quantities E_{nk} and E_γ were assumed to be independent of mass and given the approximate values $E_{nk} \approx 1.2$ Mev, $E_\gamma \approx 7.5$ Mev. The averages were taken over a Gaussian charge distribution with an rms deviation of 0.7 charge unit. Using the mass formula of Cameron,[3] $\langle E_B\rangle$ was found at the point where $\langle E_R\rangle$ had its maximum value. These quantities have been calculated for 25 fissioning species between Ra^{226} and Fm^{254} using an IBM-709 computer. However, the principal difference between the E_K calculated here and those done previously lies in the selection of ν. It was assumed that ν depends only on the mass of the fragment and not on the fissioning nuclide. This may be seen to be a good assumption by looking at the values of ν calculated by Terrell.[4] Accordingly, a smooth curve was drawn through Terrell's family of curves. The values of $\bar{\nu}$ given by this smooth curve are 2.50, 2.63, 2.86, and 3.81 for U^{233}, U^{235}, Pu^{239}, and Cf^{252}, respectively. This procedure makes ν available for all masses between 82 and 159 with the exception of the region 120 to 130. In this region the two ends of Terrell's curve were joined by a straight line. At first sight this may seem to be a very shaky business but, in fact, almost any interpolation between Terrell's two curves will do since in U^{235} (for example) it affects the shape of the kinetic energy between mass 130 and 118 but not the value at these two masses. There would still be a drop of nearly 40 Mev, even if ν were taken as identically zero for the region 121-130.

The total excitation energies at symmetry predicted by this picture are large, about 48 Mev for U^{235} and about 6 neutrons would be expected. The existence of two types of fission—symmetric fis-

sion with highly excited fragments of low kinetic energy and asymmetric fission with moderately excited fragments of high kinetic energy—might be associated with the existence of two barriers and two saddle-point configurations in the liquid drop calculations of Cohen and Swiatecki.[5] The height of the second barrier relative to the first falls rapidly as x increases above a critical value in the vicinity of 0.7 and its relatively low energy and apparent stability against asymmetry[5] suggest identifying this barrier with symmetric fission.

All three of the fissioning species showed fine structure in the mass yield between masses 134 and 146. This fine structure shows up in the total yields[6] but it is perhaps more instructive to look at the contour diagram, Fig. 2. Here it is clearly seen that the structure appears predominantly at high kinetic energies.[7] It seems to be more a result of inhibition than of preference and must be closely related to the fact that the events in this region are "running out of energy" so that the nuclei formed are nearly in their ground states. The contours along the northeast face of the mountain are nearly parallel to the line of maximum energy release. The structure is less pronounced in Pu^{239} and scarcely discernible in Cf^{252}. In these cases the mountain is further away from the limiting energy.

A full account of this work will shortly be submitted to the Canadian Journal of Physics. I am indebted to Dr. W. J. Swiatecki for pointing out the connection with the liquid drop calculations.

---

*On leave of absence from Atomic Energy of Canada Limited, Chalk River, Ontario, Canada.

[1]J. C. D. Milton and J. S. Fraser, Phys. Rev. 111, 877 (1958).

[2]J. S. Fraser and J. C. D. Milton, Nuclear Instr. 2, 275 (1958).

[3]A. G. W. Cameron, Can J. Phys. 35, 1021 (1957).

[4]James Terrell, Bull. Am. Phys. Soc. 6, 16 (1961); and private communication.

[5]S. Cohen and W. J. Swiatecki, Aarhus University Report, January, 1961 (unpublished).

[6]J. C. D. Milton, Proceedings of the International Conference on Nuclear Structure, Kingston, Canada, edited by D. A. Bromley and E. W. Vogt (University of Toronto Press, Toronto, 1960), p. 866.

[7]This is also shown in the work of W. M. Gibson, T. D. Thomas, and G. L. Miller, preceding Letter [Phys. Rev. Letters 7, 65 (1961)].

DEUTERONS FROM HIGH-ENERGY PROTON BOMBARDMENT OF MATTER

S. T. Butler and C. A. Pearson

The Daily Telegraph Theoretical Department, School of Physics, University of Sydney, Sydney, Australia

(Received June 16, 1961)

The mass analysis of the secondary particles from targets exposed to the 25-Bev proton beam of the CERN proton synchrotron has revealed an appreciable fraction of high-energy deuterons.[1] In addition large numbers of deuterons have been reported among the "grey" tracks in nuclear emulsions.[2-4]

Recently Hagedorn[5] has suggested that these deuterons are produced in elementary nucleon-nucleon collisions. However, the results obtained from a statistical model are strongly energy dependent and especially at lower energies it is hard to reconcile them with the experimental results. For deuterons with momenta below 2 Bev/c they disagree with experiment by a factor greater than 10^3.

In interpreting the emulsion results the Bristol group suggested that the deuterons are formed when a knock-on nucleon pairs with a nucleon in the tail of the Fermi distribution of the excited nucleus. Because of their high energy, however, it seems more likely that they result from the pairing of two cascade nucleons. The angular distribution of the knock-on "shower" nucleons has a strong forward peak and in many cases there will be pairs of particles which have small relative momenta. It is from such pairs that we believe deuterons are formed.

To calculate the ratio of deuterons to protons expected from such a process, we have considered the following model. An incident beam of free protons and neutrons is scattered by an effective nuclear potential, which represents the interaction of the high-energy cascade nucleons with the remainder of the nucleus. The protons and neutrons can interact with each other during the scattering. The incident particles are not parallel or monoenergetic, but have a certain momentum distribution, say $P(\vec{k})d\vec{k}$, which is the same for neutrons and protons and fits the experimental distribution for cascade protons. The flux of particles in the incident beam is chosen to yield n_0 nucleons of each type contained in the nuclear volume at any one time, where n_0 is the experimental average number of high-energy protons from a struck nucleus.

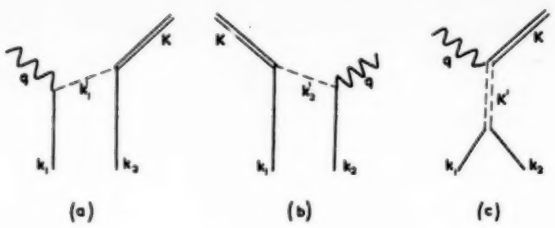

FIG. 1. Diagrams (a), (b), and (c) of Fig. 1 illustrate the simplest methods of deuteron formation. $\vec{k}_1, \vec{k}_2$ are the momenta of the proton and neutron in the initial state, $\vec{q}$ the recoil of the nucleus, and $\vec{K}$ the deuteron momentum in the final state. In case (a) the proton is scattered into an intermediate state by an interaction with the nucleus. The scattered proton and an unscattered neutron then interact with each other to form a deuteron. In case (b) a scattered neutron pairs with an unscattered proton. In case (c) the neutron and proton interact first with each other to form an intermediate deuteron state. This deuteron is then scattered by the nucleus into the final state.

To form a deuteron, a proton and a neutron must interact with each other and with the nuclear field, so that in terms of Feynman-like diagrams the simplest schemes of deuteron production can be illustrated as in Fig. 1. Here $\vec{k}_1, \vec{k}_2$ represent the momenta of the proton and neutron, $\vec{K}$ the deuteron momentum, and $\vec{q}$ the recoil of the nucleus. In diagrams (a) and (b) one of the nucleons has been scattered before the two interact to form a deuteron; in (c) they interact first with each other and the virtual deuteron formed is scattered into the final state.

The contribution from these diagrams has been calculated using a relativistic second order perturbation theory developed for this problem which will be described in a later paper. In the relativistic region the free-particle states are represented by the positive-energy solutions of the Klein-Gordon equation and the nuclear field by the effective potential calculated by Duerr[6] for such particles. In the nonrelativistic region the nucleus is represented by the well-known optical potential.

Since the formation of deuterons arises only from pairs of particles with small relative momenta, the interaction between the neutron and proton can be represented in their c.m. frame by the ordinary deuteron potential.

To simplify the calculation we have chosen $\vec{K}$ to be in the forward direction, and for comparison with the experimental results we have calculated the ratio of the number of deuterons expected in a solid angle $d\Omega$ about $\vec{K}$ with the number of free protons of momentum K which have passed through the nuclear potential and which emerge in the same solid angle $d\Omega$.

In the calculation the following parametric form for the momentum distribution $P(\vec{k})$ was chosen:

$$P(\vec{k}) \propto k^{-\alpha} (\cos\theta)^{\beta}, \qquad (1)$$

where α and β are parameters and θ is the angle of the vector $\vec{k}$ with respect to the direction of the incident nucleon which initiates the nucleon shower. This momentum distribution is normalized such that the average number of nucleons of each type within the nuclear volume at any one time, and of momenta exceeding a minimum value k_0, is the number n_0. In the CERN experiment, for example, the high-energy "cascade" protons have energies mostly exceeding 500 Mev, and their momentum distribution above this energy can be fitted by a distribution of type (1); in this case therefore we choose k_0 to correspond to an energy of 500 Mev.

In general, from an accumulation of experimental emulsion observations[4,7-10] the parameter values listed in Table I were chosen. The values of n_0 in this table refer to the silver and bromine nuclei of emulsions and would be expected to vary somewhat with the size of the nucleus.

Table I. Values of the parameters α, β, and n_0 for different minimum energies in the nucleon cascade. These values have been chosen from an accumulation of experimental emulsion observations.[a]

Minimum energy $(\hbar^2 k_0^2/2m)$ in the nucleon cascade	α	β	n_0	Range of deuteron energies calculated
30 Mev	3.5	1	6	60-250 Mev
125 Mev	3.5	2	4	250-500 Mev
250 Mev	4	3	2	>500 Mev

[a]See references 4, 7-10.

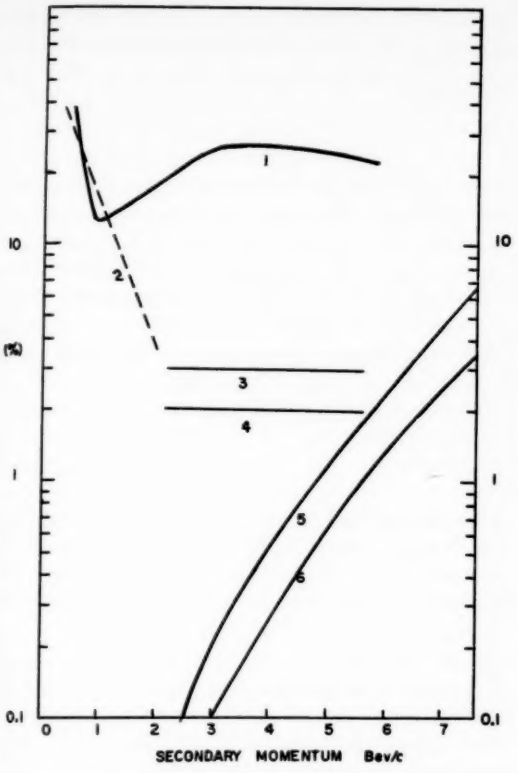

FIG. 2. A comparison of the observed and calculated deuteron to proton ratio for protons and deuterons of the same momentum. Curve 2 represents the experimental results from emulsions.[2-4] Curves 3 and 4 are the deuteron to proton ratios found in the CERN experiment. Curves 5 and 6 are the results calculated by Hagedorn for the two different deuteron factors $\Omega_d = 0.2$, 0.1, respectively. Curve 1 represents the deuteron to proton ratio calculated from the model described above.

The results of this calculation are plotted in Fig. 2 and compared with the experimental results of emulsion groups and the CERN group. The important conclusion is that there are ample numbers of deuterons formed by this process to account for the experimental observations. Indeed, in the high-energy region the numbers yielded by the present calculation are considerably too large; this is almost certainly due to the large repulsive Duerr potential[6] which we have simply taken at face value. The deuteron ratio is proportional to the square of the modulus of the effective nuclear potential, and is therefore quite sensitive to this potential. It would in fact be possible that the present deuteron formation mechanism can be used to provide a direct and sensitive measurement of the strength of the effective nuclear potential for relativistic particles.

The results of Hagedorn[5] are also shown in Fig. 2 for comparison purposes. It is difficult to reconcile the strong energy dependence of this model with the rather slow energy variation of the experimental results. Moreover, it appears to the present authors extremely probable that the statistical model employed by Hagedorn would strongly overestimate the deuterons produced in elementary nucleon-nucleon collisions at all energies, thereby impairing the "local" high-energy agreement of Hagedorn results with experiment.

In the CERN experiment moreover the percentage of deuterons detected increases with the size of the target nucleus roughly as the nuclear radius. If the deuterons are produced in nucleon-nucleon collisions, this is difficult to explain. On the present model involving the recombinations of cascade nucleons themselves such an increase of the deuteron ratio with the size of the target nucleus is to be expected.

Full details of the present calculation will be described in a later paper.

The authors are grateful to Professor Messel for providing the excellent research facilities of the School of Physics. One of us (C.A.P.) is the holder of a University of Sydney Research Studentship.

---

[1]V. T. Cocconi, T. Fazzini, G. Fidecaro, M. Legros, N. H. Lipman, and A. W. Merrison, Phys. Rev. Letters 5, 19 (1960).

[2]U. Camerini, J. H. Davies, P. H. Fowler, C. Granzinetti, H. Muirhead, W. O. Lock, D. H. Perkins, and G. Yekutieli, Phil. Mag. 42, 1241 (1951).

[3]C. Dahanayake, P. E. Francois, Y. Fujimoto, P. Iredale, P. J. Waddington, and M. Yasin, Nuovo cimento 1, 888 (1955).

[4]C. F. Powell, P. H. Fowler, and D. H. Perkins, The Study of Elementary Particles by the Photographic Method (Pergamon Press, New York, 1959).

[5]R. Hagedorn, Phys. Rev. Letters 5, 276 (1960).

[6]H. P. Duerr, Phys. Rev. 103, 469 (1956); Phys. Rev. 109, 1347 (1958).

[7]G. V. Khrimian, J. Exptl. Theoret. Phys. (U.S.S.R.) 35, 1076 (1958) [translation: Soviet Phys. - JETP 35(8), 752 (1959)].

[8]See reference 4, p. 449.

[9]K. I. Alekseeva and N. L. Grigorov, J. Exptl. Theoret. Phys. (U.S.S.R.) 35, 599 (1958) [translation: Soviet Phys. - JETP 35(8), 416 (1959)].

[10]R. R. Daniel, N. Kameswara Rao, P. K. Malhotra, and Y. Tsuzuki, Nuovo cimento 16, 1 (1960).

POSSIBILITY OF A 4-PION STRUCTURE IN THE $T=J=1$ PION-PION SCATTERING AMPLITUDE

V. De Alfaro

Istituto Nazionale di Fisica Nucleare, Sezione di Torino, Italia

and

B. Vitale

Istituto Nazionale di Fisica Nucleare, Sezione di Roma, Italia and Istituto di Fisica dell'Università, Roma, Italia

(Received May 23, 1961)

Evidence has been accumulating of late on the existence of an enhanced or resonant energy region in the $T=J=1$ pion-pion scattering amplitude. This evidence comes mainly from the analysis of the vector part of the nucleon form factors[1-3] and from a fit of the low-energy pion-nucleon "small" phase shifts, in the combination $f_{1/2}-f_{3/2}$.[4-6] The qualitative agreement about the existence of such a resonant state has not been followed yet by a quantitative agreement about its location and width that, on the contrary, have been spanning a large range, depending on the authors and on the experiment analyzed. We wish to point out here that there could exist a structure effect, due to an enhanced 4-pion state, that could possibly account for the observed discrepancies and that could in principle be observed directly in production experiments.

Let us analyze briefly how the many-pion configurations can be influenced by a resonance in the antisymmetric (both in isobaric spin and in configuration space) $T=J=1$ state. As we are mainly concerned with the possible contribution of such many-pion states to the nucleon form factors, we shall limit ourselves to the analysis of the many-pion "clouds" ($T=0$ or 1).[7] The easiest way to describe the configuration of a "cloud" is by means of Young diagrams.[8] As the total wave function of the cloud has to be symmetric, we can limit ourselves to the analysis of the configurations in isobaric space; an identical Young diagram will describe the state in configuration space. By using the notation in reference 7, the following results can be readily obtained:

$n=3$: the maximum number of $T=J=1$ pion-pion bonds ("bi-pions") is present in the configuration (111), represented by Fig. 1(a). This configuration contains three bonds, and has $T=0$ and $J=1$; it coincides with the enhanced 3-pion state discussed by Chew.[9] We shall call it, in what follows, the "three-pion."

$n=4$: the maximum number of "bi-pions" is present in the configuration (211), represented by Fig. 1(b). It contains three bonds, has $T=1$ and J odd; it can be described as a "three-pion" plus a spare pion, which leads to an immediate understanding of its $T=1$. In its lowest angular momentum state it has the same quantum numbers as the $T=J=1$ "bi-pion."

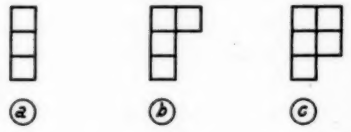

FIG. 1. Young diagrams for some of the many-pion configurations.

$n=5$: the maximum number of "bi-pions" is present in the configuration (221), represented by Fig. 1(c). It contains four bonds, and has $T=1$ and J even. The configuration (311), which has $T=0$ and J odd, contains only three "bi-pions."

It is clear from what precedes that should the "three-pion" state turn out to be strongly resonant or even bound, the 4-pion configuration (211) could play a determining role in the $T=J=1$ pion-pion scattering amplitude, where it would present itself as a second resonance or broad enhancement. Recent investigations on the scalar part of the nucleon form factors,[3] together with the results obtained by Abashian et al.,[10] strongly suggest the $T=0$, $J=1$ configuration ("three-pion" to be resonant at very low energy or, indeed, bound. It is also clear that the 5-pion (221) configuration, which can be described as a "three-pion" plus a "bi-pion," cannot give trouble in the analysis of the vector part of the form factors, having an even J; while the (311) configuration, that could contribute to the scalar part of the form factors, is probably a much weaker configuration.

Having thus established that the existence of a "bi-pion" plus that of a resonating or bound "three-pion" makes the (211) $T=J=1$ "four-pion" an interesting object to investigate, we have tried to understand what information on the "four-pion" could be inferred from the knowledge of the resonance (or binding) energies of the "bi-pion" and the "three-pion." This is a quite standard prob-

lem in low-energy nuclear physics, where at least for small values of A one wants to be able to predict something about the ground state of nucleus A by using experimental information about the nucleus $A-1$ plus one's knowledge of the forces between individual nucleons. It is quite a difficult and involved problem there, and it is even more difficult and involved in our case, of course, as we have no reliable "potential" which could describe the pion-pion interaction and therefore permit some sort of variational calculation for the 4-pion state. We have, however, made an attempt in this direction by using the so-called projection theorem, in the form recently used by Iwao et al.,[11] and applied by them to very light nuclei. We are fully aware of the fact that, since the "bi-pion" is only a resonance and not a bound state, the definition of an average kinetic energy for the infinite shell that we are filling with pions is, at best, a doubtful one. Anyway, we give our results here, with the hope that they could indicate at least qualitatively what is the influence of the "bi-pion" and the "three-pion" on the "four-pion." It is clear that the (211) 4-pion configuration in its lowest angular momentum state ($J=1$) can be most conveniently described as some kind of hydrogen-like state of a pion in S wave with respect to a "three-pion." If we now disregard the contribution (positive or negative) to the binding energy of the system coming from this S-wave interaction, we are left with only two parameters, namely: the mass of the "bi-pion," $t_V^{1/2}$, and that of the "three-pion," $t_S^{1/2}$. The projection theorem applied to this simple model gives, for the mass of the "four-pion," $t_V'^{1/2}$:

$$t_V'^{1/2} = t_V^{1/2} + \tfrac{2}{3} t_S^{1/2}. \qquad (1)$$

Let us make now the most optimistic assumption on the mass of the "three-pion," namely, let us identify it with the "particle" observed in reference 10; this gives $t_S = 5\mu^2$ and therefore:

$t_V = 22\,\mu^2$	$16\,\mu^2$	$12\,\mu^2$	$9\,\mu^2$
$t_V' = 38\,\mu^2$	$30\,\mu^2$	$25\,\mu^2$	$19\,\mu^2$

(2)

It is clear from (2) that the 2-pion cut used in references 1-6 and approximated by a narrow Breit-Wigner formula or at least by a very enhanced bump, could present on the contrary a well-defined structure (as the probable widths are smaller than the predicted separation of the bumps) and, what is more important, that the first of the two bumps (corresponding to the "bi-pion") could also span a region corresponding to a much smaller t_V than the values assumed at present. There is no real need for this enhancement to be really a very sharp resonance (see, for instance, reference 6); what matters here is that the "bi-pion" contribution could begin at lower energy and be followed by a "four-pion" contribution at higher energy. The actual determination of the parameters of an "equivalent" single resonance (up to now, attributed only to the "bi-pion") could then be strongly sensitive to the method used for estimating its contribution to the particular physical process studied, to the number of subtractions used in the representation of the physical amplitudes, and so on. This could perhaps offer one of the many possible justifications for the discrepancies found so far by the various authors in the determination of t_V.[1-6]

We note here that our neglect of the S-wave interaction can find some justification in the observational evidence for the absence of a (300) 3-pion configuration which has $T=1$ and contains only symmetric 2-pion bonds.[10]

It is obvious that production experiments, analogous to that by Abashian et al.[10] with production of H^3 and at higher energy, could directly demonstrate the suggested two-bump behavior of the pion-pion $T=J=1$ scattering amplitude. Of course, this has nothing to do with the bump which is observed at present at a much lower energy, and which can be interpreted as the "three-pion" or, alternatively, as an S-wave pion-pion effect with $T=0$.[12] The second alternative, that would leave only the form factor analysis as an indication for the existence of the "three-pion,"[3] seems, however, in strong contradiction with the most recent experiments on production of pions by pions on protons,[13] where no indication of a $T=0$ (S-wave) state was found and where the evidence is for a strongly preferred $T=1$ production. Pion-production experiments, if analyzed by means of the extrapolation procedure,[14] could indeed lead to a direct determination of the pion-pion cross section; they contain, however, a mixture of $T=0$, 1, and 2 states (although charge ratios clearly indicate a preferred production of $T=1$ states) and a mixture of angular momentum states, which makes the interpretation of the results not completely reliable. To this difficulty has to be added the well-known dif-

ficulty of obtaining unambiguous answers from an extrapolation procedure. At best, this gives indications of the general features of the process analyzed; to get more refined details and structure indications from the experimental data would require much more complete experiments than those available at present.

Useful conversations with Professor M. Cini are gratefully acknowledged. One of us (V.D.A.) wants also to thank warmly the Istituto di Fisica di Roma for the hospitality extended to him.

---

[1]W. Frazer and J. Fulco, Phys. Rev. Letters 2, 365 (1959).

[2]W. Frazer and J. Fulco, Phys. Rev. 117, 1609 (1960).

[3]S. Bergia, A. Stanghellini, S. Fubini, and C. Villi, Phys. Rev. Letters 6, 367 (1961).

[4]F. J. Bowcock, W. N. Cottingham, and D. Lurié, Nuovo cimento 16, 918 (1960); Nuovo cimento 19, 142 (1961); Phys. Rev. Letters 5, 386 (1960).

[5]S. Frautschi, Phys. Rev. Letters 5, 159 (1960).

[6]J. Hamilton, P. Menotti, T. D. Spearman, and W. S. Woolcock, Nuovo cimento 20, 519 (1961).

[7]A. Pais, Ann. Phys. 9, 548 (1960).

[8]Young diagrams were first applied to the study of the 3-pion configuration by D. Amati and B. Vitale, Nuovo cimento 2, 719 (1955); a very extensive application to the general case of n-pion "clouds" has been given by Pais, reference 7.

[9]G. Chew, Phys. Rev. Letters 4, 142 (1960).

[10]A. Abashian, N. E. Booth, and K. M. Crowe, Phys. Rev. Letters 5, 258 (1960).

[11]S. Iwao, F. B. Wang, and F. Morin, Atomic Energy Commission Report NYO-9536 (to be published).

[12]T. N. Truong, Phys. Rev. Letters 6, 308 (1961).

[13]J. A. Anderson, V. X. Bang, G. Burke, D. D. Carmony, and N. Schmitz, Phys. Rev. Letters 6, 365 (1961); A. R. Erwin, R. March, W. D. Walker, and E. West, Phys. Rev. Letters 6, 628 (1961); D. Stonehill, C. Baltay, H. Courant, W. Fickinger, E. C. Fowler, H. Kraybill, J. Sandweiss, J. Sanford, and H. Taft, Phys. Rev. Letters 6, 624 (1961).

[14]G. Chew and F. Low, Phys. Rev. 113, 1640 (1959).